NATIONAL ADVISORY COMMITTEE FOR AERONAUTICS

TECHNICAL NOTE 4243

AN EXPERIMENTAL STUDY OF THE TURBULENT BOUNDARY LAYER ON A SHOCK-TUBE WALL

By Paul B. Gooderum

Langley Aeronautical Laboratory
Langley Field, Va.

Washington
June 1958

NATIONAL ADVISORY COMMITTEE FOR AERONAUTICS

TECHNICAL NOTE 4243

AN EXPERIMENTAL STUDY OF THE TURBULENT BOUNDARY LAYER ON A SHOCK-TUBE WALL

By Paul B. Gooderum

SUMMARY

Interferometric measurements were made of the density profiles of an unsteady turbulent boundary layer on the flat wall of a shock tube. The investigation included both subsonic and supersonic flow (Mach numbers of 0.50 and 1.77) with no pressure gradient and with heat transfer to a cold wall. Velocity profiles and average skin-friction coefficients were calculated. Effects on the velocity profile of surface roughness and flow length are examined.

INTRODUCTION

In the application of the shock tube as a high-temperature test facility, a knowledge of the physical characteristics of the time-dependent boundary layer on the shock-tube wall is desirable since skin-friction and heat-conduction effects can be such as to alter the resulting flow from that predicted by ideal-flow theory. The theoretical methods by which these effects can be calculated for a turbulent boundary layer involve the assumption of a specific velocity profile, and there is very little experimental data in the literature upon which to base this assumption. Recently, subsonic velocity profiles of shock-induced flow on rough surfaces have been measured by means of a bullet technique (ref. 1). Mach-Zehnder interferometer studies of the boundary-layer growth on shock-tube walls have been reported in references 2 and 3 for shock-tube flows with low subsonic and supersonic free-stream velocities, respectively, but no attempts were made therein to calculate the velocity or other pertinent parameters from the measured density distributions. An interferometric investigation of boundary-layer velocity profiles in shock-tube flow was conducted at both subsonic and supersonic free-stream velocities in reference 4, but was restricted to the study of the laminar portion of the flow.

The purpose of the present investigation was, therefore, the interferometric study of the turbulent-boundary-layer characteristics in both a subsonic ($M = 0.50$) and a supersonic ($M = 1.77$) shock-induced flow. The

shock-tube flow under consideration was essentially an unsteady flow over a smooth flat plate with no pressure gradient and with heat transfer from the fluid to a cold wall. Also included were the effects of an evenly distributed, fine roughness.

In this investigation, the part of the boundary layer studied was the outermost or fully turbulent portion, which comprises approximately 80 percent of the total thickness. A study which would include the laminar and buffer sublayers would be very desirable since these regions are more directly affected by the wall skin friction and heat transfer. Unfortunately, in an optical study of a flow over a cold wall such as this, the light rays closest to the wall are strongly refracted toward the surface of the wall and the interferometer is thereby prevented from "seeing" this region of the fluid. The present method, however, appears to be the most promising approach to the study of boundary-layer flow of such short duration.

As in any investigation of turbulent boundary layers, before any comparison of results with theory or with other experimental data can be made, the location and stability of the transition point must be determined. It will be shown that this problem is of major concern.

SYMBOLS

A constant in equation (3), $\sqrt{\dfrac{\frac{\gamma - 1}{2} M_2^2}{\frac{T_w}{T_2}}}$

B constant in equation (3), $\dfrac{1 + \frac{\gamma - 1}{2} M_2^2}{\frac{T_w}{T_2}} - 1$

C_F average skin-friction coefficient, $\frac{1}{\xi} \int_0^{\xi} c_f \, d\xi$

c_f local skin-friction coefficient, $\dfrac{\tau_w}{\frac{1}{2} \rho_2 u_2^2}$

c_p specific heat at constant pressure

F	constant
H	boundary-layer form parameter, δ^*/θ
k	Gladstone-Dale constant
K	compressibility correction
L	length of light path through the disturbance in the test section
l	correction applied to path length L to account for the side-wall boundary-layer and corner effect
M	Mach number
N	reciprocal of velocity exponent in the equation $\frac{u}{u_2} = \left(\frac{y}{\delta}\right)^{1/N}$
p	local pressure
R	Reynolds number based on flow length along plate, $u_2\xi/\nu_2$
S	fringe shift (dimensionless)
t	time
T	absolute temperature
u	velocity relative to the wall
W	internal width of the test section
x	coordinate measured parallel to the shock-tube axis
y	coordinate measured perpendicular to the bottom shock-tube wall
z	coordinate measured perpendicular to the shock-tube axis and parallel to the bottom shock-tube wall
γ	ratio of specific heat at constant pressure to specific heat at constant volume, assumed to vary with temperature
δ	thickness of the boundary layer

δ^* boundary-layer displacement thickness, $\int_0^\delta \left(1 - \frac{u}{u_2}\right) \frac{\rho}{\rho_2} dy$

θ boundary-layer momentum thickness, $\int_0^\delta \left(1 - \frac{u}{u_2}\right) \frac{u}{u_2} \frac{\rho}{\rho_2} dy$

μ coefficient of viscosity

ν kinematic viscosity

$\bar{\tau}_w \Big|_a^b$ average local shearing stress between points a and b on x,t diagram

λ wavelength of light in a vacuum

ξ free-stream flow length

ρ density

τ local shearing stress

$$\Psi = \frac{1}{2} KF\left(\frac{u_2}{\nu_2}\right)^{-2/(N+3)} \Omega^{-(N+1)/(N+3)}$$

$$\Omega = 1 + \frac{u_s}{u_s - u_2}\left(\frac{\delta^*}{\theta} - 1\right)$$

Subscripts:

o reference point on θ,ξ curve

1 region ahead of shock wave

2 uniform-flow region behind shock wave

a,b points on x,t diagram

n any light ray through the boundary layer

s shock wave

w wall

δ outer edge of boundary layer

trans transition

∞ free stream

A bar over a symbol indicates the mean value.

APPARATUS

Shock Tube

The studies of the boundary-layer development were made in a stainless-steel shock tube of rectangular cross section, 4 inches wide and $7\frac{1}{2}$ inches high, designed for a maximum internal pressure of 100 pounds per square inch. The bottom wall of the shock tube, a ground and polished surface on which the boundary layer was studied, had three joints located 1.1, 3.1, and 7.1 feet upstream of the vertical reference wire in the test section. Dowels between the shock-tube sections insured accurate alinement of these joints. This wall was later completely covered with artificial roughness, consisting of very closely spaced No. 160 carborundum grains. These were lacquered over 7 feet of the length of the wall upstream of the vertical wire in the test section. The experimental arrangement is diagramed in figure 1.

The high-pressure section was 4 feet long and had a rod of 7/16-inch diameter running lengthwise through its center to puncture the diaphragm at a predetermined pressure. Rectangular diaphragms of 2024-0 aluminum alloy (0.032 inch thick) were scribed diagonally on the low-pressure side to such a depth that the diaphragm would be close to its breaking point at the particular pressure of each run. Air at 60 pounds per square inch and helium at 100 pounds per square inch, both at room temperature, were used in the high-pressure chamber. The diaphragms were placed so that the rod would make its puncture at the intersection of the scribe marks.

The low-pressure end was made up of five separate sections, two of which contained 8- by 18-inch glass side walls 1.2 inches thick. The first of the two sections with glass side walls extended between 12 and 14 feet from the diaphragm and was traversed by the light beams for the shock-velocity measuring stations. The second extended between 14 and 16 feet from the diaphragm and contained the test section with windows of select plate glass, interferometer light beam, and associated reference wires. With air at 60 pounds per square inch gage in the high-pressure end, the low-pressure side of the shock tube was at room conditions; with helium at 100 pounds per square inch gage in the high-pressure end, the low-pressure end was evacuated to approximately one-fiftieth of an atmosphere (15.1 mm Hg abs).

Interferometer

The interferometer was of the Mach-Zehnder type and straddled the tube at the midpoint of the test section. Its field of view was 3 inches square. The light source was a spark obtained by discharging a 0.25-microfarad capacitor, charged to 16,000 volts, across an air gap between two magnesium electrodes. The light from the spark illuminated the entrance slit of a monochromator set to pass the magnesium triplet at a wavelength of 5,170 angstroms. The exit slit was parallel to the fringes and measured 0.25 mm by 2 mm.

The objective of the interferometer camera was an f/5 parabolic mirror of 30-inch focal length. The light from this mirror was reflected off-axis so that the focal point of the reflected beam would be located outside the incoming beam. The camera was focused halfway across the span of the boundary-layer plate at $\frac{1}{2}$ W. However, because of the resultant astigmatism, the point of best focus varied from $\frac{1}{3}$ W for vertical lines to $\frac{2}{3}$ W for horizontal lines, measured from the camera side of the shock tube in white diffuse illumination. The magnification of the camera was 0.28.

Light Screens

The shock velocity was measured optically by means of two light screens, spaced 12.78 inches apart. The second station was located 19.09 inches upstream of the vertical reference wire in the test section. Each beam was 2 inches high by 0.02 inch wide. The light source for each system was a 10-watt concentrated arc lamp and the sensitive element was a 931A photomultiplier. The time required for the shock wave to traverse the distance between the light screens, as well as the time between the tripping of the second light screen and the taking of the interferogram, was recorded on electronic counter-chronographs.

EXPERIMENTAL PROCEDURE

The technique of observing the diffraction fringes of a wedge placed in the interferometer's field of view in the test section was used to adjust the interferometer so that its beam of light was accurately parallel to the bottom wall of the shock tube. The camera of the interferometer was then focused midway between the shock-tube windows. The no-flow fringes were oriented perpendicular to the bottom surface of the shock tube. This arrangement, in contrast to parallel fringe orientation,

permitted not only an easier evaluation of the equations required to obtain the fringe-shift gradient normal to the wall but also a better determination of the outer edge of the boundary layer.

The experimental procedure was similar for the high-speed and low-speed tests. Either dry bottled air or helium at room temperature was admitted into the high-pressure chamber and the low-pressure end was adjusted to the correct pressure, after which the diaphragm was broken by the rod. The shock wave moving through the low-pressure chamber was timed, and the flow following the shock was photographed at a predetermined instant. Both interferometer and schlieren pictures were taken of the flow, but they could not be taken at the same time. One flow photograph could be made during each run by adjusting the variable time delay to such a setting that all the data lay within the uniform flow of region 2 shown on the x,t diagrams of figure 2. The boundary-layer growth was then determined from a series of photographs taken at successive time intervals after the shock wave passed the center of the test section.

The free-stream flow conditions behind the shock wave (region 2) were determined by using the conditions ahead of the shock (region 1) and the shock velocity in the Rankine-Hugoniot relations for the flow through a shock with γ variable.

Interference photographs of the boundary layer, shown in figures 3(a) and 3(b) are typical of the low- and high-velocity runs with a smooth wall. The density gradient in the boundary layer is indicated by a displacement of the interference fringes from the uniform-flow position in the free stream. In these figures, a displacement to the right indicates an increase in density. Although the total fringe shift at the wall is approximately the same (20 to 21 fringe widths) for both the high- and the low-velocity free-stream flow cases, a shift of only 2 widths is visible in the supersonic flow as compared with 7 or 8 in the subsonic flow. The flow is from left to right; flow length is therefore increasing from right to left and is defined as the distance a free-stream particle has moved since it was set in motion by the shock. The equation for the ratio of flow length to shock-tube length is

$$\left|\frac{d\xi}{dx}\right| = \frac{1}{\frac{u_s}{u_2} - 1}$$

In the low-speed case (fig. 3(a)), the difference in flow length between particles located in the free stream on opposite sides of the picture is 0.17 foot; in the high-speed case (fig. 3(b)) this difference is 1.10 feet. The width of both pictures, measured in shock-tube coordinates,

is 0.25 foot. The gradual curve of the interference fringes in the free-stream region above the boundary layer occurs in both the no-flow and the flow photographs, and therefore should not be interpreted as a density gradient in the free stream. It is due, instead, to the imperfection of the shock-tube windows. Average values of various flow parameters for both the subsonic and the supersonic cases are given in table I.

A schlieren survey of the region of flow covered by the interferograms was also made. Typical schlieren photographs of the shock waves and of the region immediately behind them are reproduced in figures 4(a) and 4(b) for the low- and high-velocity flow over a smooth wall.

The interferograms were analyzed by the method of superposing with-flow and no-flow interferograms (ref. 5). The measurement of the fringe shift was accomplished as follows: A photographic print of the interferometric negative was made approximately four times actual size. Six to eight cross sections (i.e., positions along the wall) on each interferogram were measured directly on the enlargement, and a plot of fringe-shift variation with distance from the surface of the plate was then obtained.

A limitation of the comparator used to measure the positions of the centers of the fringes prevented simultaneous x and y measurements. Therefore, because of the large number of cross sections processed, only values of $S = 1/2, 1, 1\frac{1}{2}$, and so forth, were measured (except for some of the high-speed data), since only the centers of the fringes can be accurately measured along a line of fixed position. If a one-dimensional flow field can be assumed, intermediate fringe shifts can be obtained, as outlined in reference 6, by determining the shape of the fringes in the region under study. This procedure was followed for only a few selected cross sections of the supersonic smooth-wall boundary layer.

The resulting fringe shifts for cross sections of approximately the same free-stream flow length were then averaged arithmetically in both ξ and y, and the average fringe shift was then related to the density by means of the following general equation, applicable to two-dimensional flow fields:

$$\rho_n = S \frac{\lambda}{Lk} + \rho_\delta \qquad (1)$$

where

$$\rho_\delta = \rho_2$$

In the calculation of the density, two corrections were applied. One correction was made to account for any slight change in the "undisturbed" fringe spacing occurring during the interval between the taking of the no-flow interferogram before the run and the taking of the flow interferogram. This correction was made in the darkroom by slightly adjusting the size of the enlargement of the no-flow interferogram so that the spacing of the fringes would coincide with the spacing of the fringes in the region of uniform density on the with-flow interferogram. At the same time, spurious fringe shifts, caused by turbulence in the side-wall boundary layer, were somewhat reduced by matching the no-flow interference fringes to the best average of those in the free stream of the with-flow picture.

The other correction, which was made to account for the effect of the side-wall boundary layers and their intersection at the lower corners of the shock tube with the boundary layer being studied (fig. 5), is derived in appendix A under the assumption that the average boundary-layer profiles at a particular value of ξ on the windows and on the bottom wall were identical. This correction is applied to the length of the light path through the test section and results in a shortening of the shock-tube width W by the amount $2(\delta - l)$. Equation (1) becomes

$$\rho_n = \frac{S\lambda}{k(W - 2\delta + 2l)} + \rho_\delta \tag{2}$$

where

$$l = \frac{\int_{y_n}^{\delta} (\rho - \rho_n)dz}{\rho_\delta - \rho_n} \tag{3}$$

The length l was found to a second approximation by assuming that the density variation through the side-wall boundary layer was that calculated from the measured fringe shift by using equation (1) and $L = W$. Then by graphical integration of the resulting plot and equation (3), l was determined to a third approximation. The process could then be repeated to obtain a fourth approximation, but the third was found to be sufficient for this particular investigation.[1] After the estimation of the corner effect on the path length, the average density profile for a particular flow length was computed from the average fringe-shift distribution and plotted as a function of the distance y/δ. (A general discussion of the assumptions made in relating the density to the fringe shift is contained in appendix B.)

---

[1]Note that for $L = W$, the first approximation to l is δ.

With conditions in the stream and the mean local fluid densities determined, it was possible to calculate the mean local velocities from the densities. With the assumption of constant pressure in the boundary layer normal to the wall, use can be made of the following relation due to Van Driest (ref. 7) for a fluid with a Prandtl number of 1.0:

$$\frac{T_w}{T} = \frac{\bar{\rho}}{\rho_w} = \frac{1}{1 + B\frac{\bar{u}}{u_2} - A^2\left(\frac{\bar{u}}{u_2}\right)^2} \tag{4}$$

where

$$A^2 = \frac{\frac{\gamma - 1}{2} M_2^2}{\frac{T_w}{T_2}}$$

$$B = \frac{1 + \frac{\gamma - 1}{2} M_2^2}{\frac{T_w}{T_2}} - 1$$

and

$$T_w = T_1$$

Equation (4) can be applied only if the assumptions are made that constant pressure exists throughout the fluid, that the Prandtl number is unity, that the boundary layer is thin, and that the specific heat of air at constant pressure is constant throughout the flow field at the value determined by the temperature of the fluid at the wall. This last assumption is a serious deviation from the truth, in the case of the supersonic free stream, since the temperature at the wall is approximately 540° R, while the temperature of the fluid in the free stream is approximately 2,500° R, and this could result in an error in the calculated velocity profile.

In the derivation of equation (4), steady turbulent flow over a stationary wall was assumed. The question arises as to whether this equation can be applied to the unsteady flow of the problem under study. In reference 8 an expression was derived for the temperature-velocity relation for a laminar boundary layer developing behind a traveling shock wave, wherein the coordinate system was allowed to move with the shock. The flow is steady in these coordinates. If this relation is

transformed to the stationary (unsteady) coordinates used herein, in its transformed state it is identical to the so-called Crocco relation. Since the Crocco relation is the same as Van Driest's equation (the only difference being that the Crocco relation was derived for a laminar boundary layer and therefore requires instantaneous values of the variables), it would appear that the Van Driest equation could also be applied to the unsteady-flow boundary layer without serious reservation.

Equation (4) also requires a knowledge of the temperature of the surface of the plate. Throughout the present calculations, the temperature of the wall is assumed to be the wall temperature measured immediately before each run. Actually, experiments with thin-film resistance thermometers (ref. 4) indicate that there is a small temperature rise on the wall with the passage of the shock wave for a smooth-wall boundary layer and another with the passage of the transition point, both of which might total several degrees at the longer flow lengths used herein. In the case of the rough wall, however, the assumption that the temperature of the small particles of carborundum imbedded in a lacquer insulator would as closely duplicate the surface temperature of a smooth steel plate under similar flow conditions is questionable. The anticipated effect of the roughness on the wall temperature is an increase in the wall surface temperature beyond that which occurred in the case of the smooth wall. As a consequence, the final velocity profile could be in error owing to the fact that the assumed temperature of the surface is too low, and this error would result in a velocity profile with a higher than actual value of N (if the profile were following the velocity law $\frac{u}{u_2} = \left(\frac{y}{\delta}\right)^{1/N}$).

Another important requirement of equation (4) is that the known density profile through the boundary layer must be a mean-value profile. In a study of a highly turbulent flow involving instantaneous pictures, the achievement of a fairly reliable mean profile would be expected to require the processing of a large number of cross sections for each combination of the free-stream flow parameters investigated. In the present investigation, because of the practical limitations of the interferometric techniques, it was possible in the highly turbulent cases to measure only a few.

The attainment of a statistical average with a minimum number of cross sections was assisted by the fact that the information from an interferometer is already an integrated result and the amount of inhomogeneity observed is a function of the narrowness of the test section and the scale of the turbulence. A hindrance was the fact that in the vicinity of the free-stream boundary the diffuseness of the fringes caused difficulty in locating points corresponding to small changes in density and contributed to the difficulty of fairing an accurate fringe-shift

curve through this region. Another difficulty was the fact that since the tests, performed at certain nominal pressure ratios, were actually made with the high-pressure chamber at the same gage pressure, variations in atmospheric pressure and temperature from run to run and variations in the manner in which the diaphragm burst made it difficult to reproduce a given state by repeated identical runs. In this investigation, all data in which the free-stream flow velocity varied from the mean by more than 1 percent were discarded. In the final analysis, after the undesired data were discarded, 141 density profiles were measured for the subsonic smooth-wall boundary layer and 488 profiles for the supersonic smooth-wall boundary layer. It was found that fewer cross sections were needed in the vicinity of transition than at the longer flow lengths.

Close behind the advancing shock wave, the boundary layer is thin and laminar in structure; a density-profile measurement is beyond the resolution of the optical equipment used to obtain the present data. Accordingly, there is no direct evidence of the beginning of transition to turbulence. Indirectly, the beginning of transition is indicated on the interferograms by a large change (decrease) in the amount of light cut off, caused by refraction. Simultaneously, a rapid increase in δ occurs. Because of disturbances present in the free stream for both the high- and low-speed flow cases, it would be dangerous to attach too much importance to the transition data as such. It is believed, however, that the characteristics of the turbulent layer are independent of the elements which caused the destruction of the laminar layer.

The outer edge of the transition region of the supersonic smooth-wall boundary layer was quite repetitious (fig. 6). At longer flow lengths, however, the repetition ended. Because of the large spread in the data in this region, an attempt to obtain a better average at one flow length resulted in the reading of 66 cross sections at values of ξ near 8.3 feet. Arithmetic averages of ξ and of y were then taken. The individual values of y which made up this mean profile were inspected at several particular values of ρ/ρ_2, and for each value of ρ/ρ_2 they were found to have an unsymmetrical distribution about the arithmetic mean, with the arithmetic mean exceeding the most probable value of y by a slight amount. Since most of the data points reported herein are arithmetic averages, it is possible that all the data resulting from such an average are likewise displaced slightly toward the stream from the true mean value. It is believed, however, that this effect is small.

RESULTS AND DISCUSSION

The principal results of this investigation are the density distributions. However, preliminary to a discussion of these profiles, a plot of the measured position of the free-stream edge of the boundary layer as a function of flow length for the various combinations of free-stream velocity and wall condition is of interest. The variations of boundary-layer thickness with flow length for the smooth wall, subsonic and supersonic cases, are presented in figures 6(a) and 6(b); for the rough wall, subsonic and supersonic cases, in figures 6(c) and 6(d).

Density and velocity profiles through the boundary layers of figure 6 are presented in figures 7 to 11. Mean profiles for four free-stream flow lengths in the fully turbulent region of the subsonic flow ($M_2 = 0.50$) over a smooth wall are shown in figure 7(a). Because the data in the transition region did not exhibit the irregularity characteristic of the longer flow lengths, a particular photograph of the transition region of this flow was chosen for evaluation, and the results were plotted as individual cross sections in figure 7(a). The curves of figure 7(a) show similarity with each other. The overall range of variation of the parameter y/δ at several density ratios is indicated in the figure by arrows. Velocity profiles, calculated from the density profiles of figure 7(a) by means of equation (4), are presented in figure 7(b).

The density and velocity profiles for the supersonic turbulent smooth-wall boundary layer were computed and are plotted in figures 8(a) and 8(b). A salient feature of these plots is the large spread in the data, which is probably due to the large scale of the turbulence. Figure 6(b) shows that this spread begins immediately behind the transition region and increases with flow length. The distributions of figure 8 are similar in the vicinity of the wall, and the spread in the data increases rapidly toward the free stream, causing an irregular variation in shape with flow length, the profile at the highest flow lengths being similar to that at the lowest.

The spread of the data that make up the average profiles of the supersonic boundary layer point up the need for much more data. Unfortunately, more time was not available for this purpose. Instead, a curve was faired through the data points of figure 6(b). A few pictures were then selected which maintained a thickness close to that of the faired curve and which had a fringe-shift profile which was reasonably close to the average of the other cross sections in the same flow-length group. These selected pictures are indicated by solid symbols (each group being those taken from a single interferogram) in figure 6(b). The selected interferograms were then reread, by the method outlined in reference 6, to obtain intermediate fringe-shift values, and the six or seven cross sections of each picture were averaged together. The resulting density and velocity profiles are

shown in figures 9(a) and 9(b) for six free-stream flow lengths, together with six individual transition profiles. This treatment improved the correlation with flow length of the high-velocity density and velocity profiles to such an extent that the curves of figure 9 can be said to show close similarity, with the exception of the cross sections of the transition region.

To find out what effect roughness would have on the density and velocity profiles and on the scatter of the data, the experiment was repeated with No. 160 carborundum powder distributed uniformly over 7 feet of the boundary-layer plate preceding the test section. No data were taken at flow lengths greater than 7 feet; and in the low-speed flow case, no data were taken in the transition region. The total height of this roughness was 0.004 inch, and the surface of the plate was raised by this amount when it was plotted on the interferograms. The resulting position of the free-stream boundary and the computed density and velocity profiles are presented in figures 6(c), 6(d), 10, and 11. An interesting result was that, although the roughness had a considerable effect on the thickness of the subsonic boundary layer, no large effect on the high-speed boundary-layer profiles was found.

The velocity profiles of figures 7 to 11 were also plotted exponentially in order to effect easy comparison with the profiles usually assumed in theoretical studies of the turbulent layer, wherein the velocity ratio is usually assumed to vary as $(y/\delta)^{1/N}$. These comparisons are shown in figures 12 to 17, where the theoretical distributions are represented by the solid and dashed straight lines, the data points by the symbols, and the overall spread in the data by arrows. The velocity profiles for the subsonic smooth-wall boundary layer (figs. 12 and 13) follow the one-seventh power law closely, and this also agrees with a velocity profile which was calculated from the data of reference 3 ($M_2 = 1.05$; $\xi = 1.4$ ft) by means of equation (4). The rough-wall data are approximated better by a one-sixth power profile.

The supersonic smooth-wall profiles in the transition region (fig. 15) fit the one-seventh power law, with the exception of the profile at the longest flow length. The profiles farther downstream in the fully turbulent portion of the boundary layer were better approximated by the one-fifth power law. The supersonic rough-wall data from the transition region (fig. 17) were not approximated very well by any straight line. Only two sets of data outside the transition region were available in this case, and both of these were for approximately the same free-stream flow length. As they produced identical profiles, only one is shown (fig. 17(e)), and this follows the one-fourth power law. It should be noted that the effects of roughness on the profile shape of both the subsonic and supersonic turbulent layers were similar and caused the profiles to shift toward a

slightly lower value of N. This is opposite to the wall-temperature effect mentioned previously.

The determination of the boundary-layer density and velocity distributions made possible the calculation of the boundary-layer parameters θ, δ^*, and H, and these are presented, along with δ, in figure 18 $(M_2 = 0.50)$ and figure 19 $(M_2 = 1.77)$. Both smooth- and rough-wall data are plotted on the same figure to facilitate comparisons. In addition, figure 19 shows the parameters calculated from both the averaged and the selected profiles.

Equations applicable to these flow conditions have been derived by Robert L. Trimpi of the Gas Dynamics Branch of the Langley Aeronautical Laboratory. From these it is possible to calculate, theoretically, the variation of momentum thickness θ with flow length ξ, by making the assumption of a power profile and using the Sommer-Short method of compressibility correction. The expression found for momentum-thickness variation is

$$\theta = \left[\theta_o^{\frac{N+3}{N+1}} + \left(\frac{N+3}{N+1}\frac{KF}{2}\frac{\nu_2}{u_2}\right)^{\frac{N+3}{N+1}}\frac{1}{\Omega}\frac{u_2}{\nu_2}(\xi - \xi_o)\right]^{\frac{N+1}{N+3}}$$

where $\theta = \theta_o$ at $\xi = \xi_o$, and

$$\Omega = 1 + \frac{u_s}{u_s - u_2}\left(\frac{\delta^*}{\theta} - 1\right)$$

If

$$\Psi = \frac{1}{2} KF\left(\frac{u_2}{\nu_2}\right)^{-\frac{2}{N+3}} \Omega^{-\frac{N+1}{N+3}}$$

and for a one-seventh-power velocity distribution $F = 0.058$, $N = 7$, and $\frac{\delta^*}{\theta} = 1.286$, then

$$\theta = \left[\theta_o^{5/4} + \left(\frac{5}{4}\right)^{5/4}\Psi^{5/4}(\xi - \xi_o)\right]^{4/5}$$

For the low-speed case $(p_2/p_1 = 2)$,

$$K = 1.05$$

$$\nu_2 = 0.00019 \text{ ft}^2\text{sec}^{-1}$$

For the high-speed case $(p_2/p_1 = 25)$,

$$K = 1.22$$

$$\nu_2 = 0.00442 \text{ ft}^2\text{sec}^{-1}$$

The resulting theoretical variation is shown in figures 18(a) and 19(a) for the condition in which the virtual origin of the turbulent layer is at $\xi = 0$ and also for the condition in which the theoretical θ is equal to the experimental θ at the end of transition. The agreement between theory and experiment in the case of the supersonic stream is not very good, especially at the longer flow lengths. This discrepancy could be due to the incorrect assumption of a one-seventh power profile, since the fully turbulent experimental profiles for this case followed more closely the one-fifth power law. The agreement between theory and experiment in the case of the subsonic stream is much better.

It was found that the boundary layer behind the shock wave was laminar for a certain distance and then suddenly became turbulent. It might be expected that the beginning of transition would vary from streamline to streamline across the span of the plate. If this were the case, since the results from the interferometer are an integrated average the resulting velocity profile should be between a typical laminar and a typical turbulent layer in shape. However, no such condition was found, as was shown by the velocity profiles at successive stations in the transition region. Neither was there a gradual change away from what would be considered a laminar shape distribution. Actually, both subsonic and supersonic transition profiles agree well with the one-seventh power law. If the points indicated in figures 6(a), (b), and (d) as the beginning of transition can be assumed to be correct, then the transition Reynolds number $u_2\xi_{trans}/\nu_2$ was 2×10^6 for the supersonic stream over both rough and smooth walls and 1.4×10^6 for the subsonic stream over a smooth wall. No transition data were obtained for the subsonic stream over a rough wall. It is believed that the transition results for the high-speed flow over a smooth wall are the most reliable because there are fewer disturbances in the stream than for the subsonic flow case, and also because, as has been suggested by various investigators, the effects of roughness elements on

the surface of a plate in supersonic flow are less important since the disturbances that are produced are propagated outside the boundary layer as compression waves. This outward propagation of disturbances may also account for the small effect of roughness on the data for high-speed fully turbulent flow.

Reference 3 (turbulent profiles) and reference 4 (laminar profiles) report density variations which decrease monotonically from the wall to the stream. Reference 2 (laminar and turbulent profiles), however, indicates a density reversal in the vicinity of the stream. The reason for such behavior of a turbulent boundary layer on a cold wall is not understood. It was established that for the visible regions of the boundary layers of both the subsonic and the supersonic free stream of the present investigation the density variation was a monotonically decreasing function of y. This finding is in agreement with references 3 and 4, and is at variance with the data of reference 2.

Values of the average skin-friction coefficient C_F were calculated from the momentum-thickness variation with ξ by means of a modified Kármán momentum equation. Consider the following sketch, in which the change in momentum thickness θ with time at x = Constant is known:

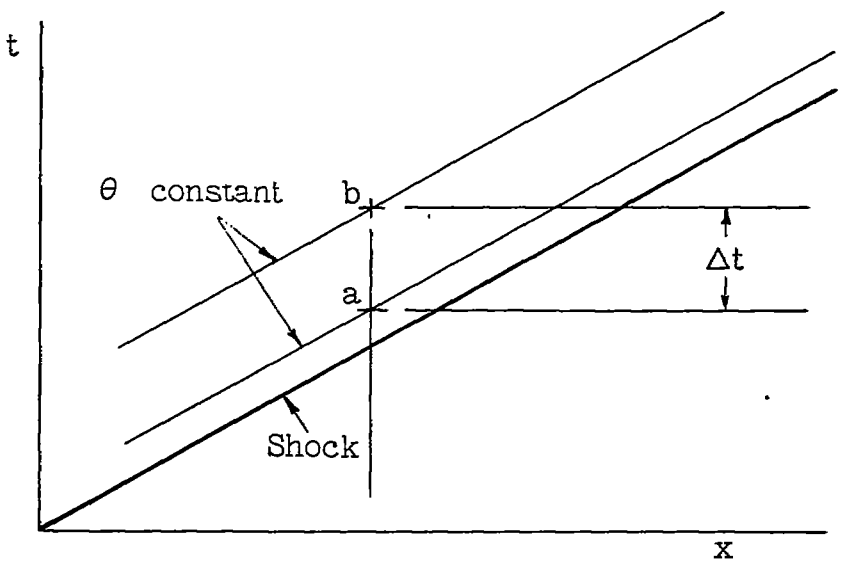

Then,

$$C_F = \frac{\bar{\tau}_w \Big|_a^b}{\frac{1}{2}\rho_2 u_2^2}$$

$$= 2\left(\frac{\partial\theta}{\partial t}\right)_x \left(\frac{1}{u_2}\frac{\delta^*}{\theta} - \frac{1}{u_s}\right) \tag{5}$$

$$= 2\,\frac{\theta_b - \theta_a}{t_b - t_a}\left(\frac{1}{u_2}\frac{\delta^*}{\theta} - \frac{1}{u_s}\right) \tag{6}$$

Equations (5) and (6) were also derived by Robert L. Trimpi. If the experimental variation of θ with ξ after transition is approximated by a straight line, and δ^*/θ is assumed to be constant over the same interval, then the values of the variables of equation (6) are as follows:

	M_2	$\frac{\delta^*}{\theta}$	$\theta_b - \theta_a$, in.	$t_b - t_a$, sec	ξ_a, ft	ξ_b, ft	C_F
Low speed; smooth wall	0.50	1.30	0.058	0.003700	0.3	4.2	0.00375
High speed; smooth wall	1.77	1.42	.030	.000409	4.7	14.1	.00173
Low speed; rough wall	.49	1.38	.035	.001982	2.1	4.2	.00470

SUMMARY OF RESULTS

The unsteady (shock-induced) boundary layers over both a smooth wall and a wall with evenly distributed roughness have been observed by means of an interferometer for subsonic and supersonic free-stream flows (Mach numbers of 0.50 and 1.77) with zero pressure gradient and with heat transfer to a cold wall. Density profiles were calculated from the average fringe-shift distributions under the assumption that there were no refraction effects, but were corrected for corner effects. The measurement of the density profiles permitted calculation of the velocity

profiles under the assumption that the Prandtl number of the fluid in the boundary layer was unity, that the specific heat of air at constant pressure was constant at the value computed for the flow at the surface of the wall, and that T_w (the temperature of the wall) was equal to T_1 (the temperature of the air in the region ahead of the shock wave). In addition to the density and velocity profiles, the results of this investigation can be summarized as follows:

1. The transition regions were readily distinguishable but their positions could be influenced by disturbances present in the flow. The transition Reynolds numbers obtained, however, were 2×10^6 for supersonic flow over a smooth wall $\left(T_w/T_2 = 0.22\right.$, where T_2 is the temperature of the air in the uniform-flow region behind the shock wave$\left.\right)$, and 1.4×10^6 for subsonic flow over a smooth wall $\left(T_w/T_2 = 0.8\right)$. The transition velocity profiles for both cases followed the one-seventh power law.

2. The mean velocity profiles in the flow following the transition region obeyed the power laws quite well, but no single law could be generally applied. Profiles at a particular Mach number and wall condition were found to be similar for various free-stream flow lengths when plotted nondimensionally.

3. Computation of the momentum thicknesses permitted comparison with theoretical smooth-wall distributions calculated from unsteady-flow theory for a one-seventh-power velocity law. The optical and the theoretical distributions show satisfactory agreement for the subsonic flow but poor agreement for the supersonic flow.

4. The main effect of the addition of roughness was to cause a substantial increase in the thickness of the subsonic layer. There was no change in the thickness of the supersonic layer. The shapes of both the subsonic and supersonic velocity profiles were affected by a corresponding but small amount.

Langley Aeronautical Laboratory,
National Advisory Committee for Aeronautics,
Langley Field, Va., January 29, 1958.

APPENDIX A

CORNER CORRECTION

In order to obtain the corner correction, the assumption was first made that at a particular value of ξ the average boundary layers on the windows and on the bottom wall were identical. The path length L of equation (1) was then corrected as follows. Consider figure 5, in which it is assumed that the boundary layers intersect discontinuously. The solid line of figure 5(a) represents the path along which the mean density variation (solid line) of figure 5(b) is experienced by a light ray that passes through the flow at the free-stream edge of the boundary layer. The dashed lines of figure 5(a), similarly, are the paths along which the density variation of figure 5(b) is experienced by a ray passing through the boundary layer at a height $y = y_n$ above the surface of the plate. Within the sections of light path δ between $z = y_n$ and $z = \delta$, the density may be assumed to vary as the dotted line instead of as the solid line. The value of l to be determined is that for which the fringe shift between ray n and ray δ with the assumed distribution will be equal to the fringe shift between ray n and ray δ with actual (solid) distribution. If the assumed distribution of the fringe shift is

$$S = \frac{lk}{\lambda}(\rho_\delta - \rho_n)$$

and the actual distribution is

$$S = \frac{k}{\lambda}\int_{y_n}^{\delta}(\rho - \rho_n)\,dz$$

then

$$l = \frac{\int_{y_n}^{\delta}(\rho - \rho_n)\,dz}{\rho_\delta - \rho_n}$$

The effective light path L of equation (1) is therefore

$$L = W - 2\delta + 2l$$

and equation (1) becomes

$$S\frac{\lambda}{k} = \left(\rho_n - \rho_\delta\right)(W - 2\delta + 2l)$$

APPENDIX B

SOURCES OF ERROR DUE TO LIMITATIONS OF THE INTERFEROMETRIC METHOD

Equation (2) can be applied only if a reference density in the flow field can be definitely established and if the fringe-shift variation through the boundary layer is representative of the assumed two-dimensional flow and can be accurately measured.

In this investigation, the free-stream flow was used as the reference condition. A schlieren survey of the flow behind the shock was therefore made to determine whether any large disturbing factors were present in the free stream of the region under study. Two of these photographs, reproduced in figure 4, show the stream immediately behind the shock to be, indeed, full of disturbances which have as their source the joints in the shock-tube wall, machining marks on the upper wall of the test section, and the diaphragm burst. However, investigation with the interferometer revealed a negligible density variation in the free stream and indicated that the disturbances visible in the schlieren survey were actually quite weak. In a sensitive schlieren system, a weak disturbance may photograph with nearly as much contrast as a much stronger wave (note the many waves due to the upper-wall machining marks, which actually were only 0.0001 to 0.0002 inch in height).

Estimates of the flow Mach number M_2 were made on the schlieren photographs by measuring the positions of the free-stream disturbances and calculating their velocity. Only in the high-velocity case did the measurements indicate that the actual flow Mach number was different from the value calculated from the shock-velocity measurements. In this case, the actual flow Mach number was consistently low by approximately 2 percent. This discrepancy could be caused by an incorrect shock-velocity measurement, by boundary-layer growth behind the shock wave, and by the associated attenuation of the shock wave. Attenuation is not believed to be a serious factor in this investigation, because in pictures of zero time delay the shock appeared at the calculated point in the test section, as determined by the shock-velocity measurement. Since the velocity of the shock wave was measurable with an accuracy of ±0.5 percent at the worst, the discrepancy in free-stream Mach number is probably due to the boundary-layer growth rather than error in determination of the speed of the shock wave. It was not practical, however, to correct the flow velocity by measurement of the disturbance velocities on schlieren photographs because of the uncertainty in these measurements.

Therefore, all calculations were based on free-stream conditions determined from the shock-velocity measurement.

A question common to most two-dimensional optical flow studies is whether a truly two-dimensional flow exists. The nonideal flow factors in the present investigation probably include, in addition to the side-wall boundary-layer effect, a variation of stream conditions and/or boundary-layer conditions along the light path for a particular cross section of the flow. The magnitude of these variations is not known, but in view of the irregular variation in a longitudinal direction of the various boundary-layer flow quantities along the wall, it is quite conceivable that some variation occurs laterally as well. Other sources of error lie in the assumptions that the boundary-layer thickness and density on the side walls are the same as on the floor of the shock tube, and that the intersection of the plate and side-wall boundary layer is abrupt, rather than with somewhat of a rounded corner fillet. These two assumptions should not result in significant errors, since the fringe shift is insensitive to disturbances of small density change and path length. The one possible exception is the effect of a corner fillet on the location of the free-stream edge of the boundary layer.

Measuring errors can usually be classified as either random or systematic. Measuring errors of a random nature have their source in the uncertainty with which comparator readings can be made of the centers of the fringes. At any one point in the flow, this error is generally accepted to be a maximum of 0.1 fringe width, which is a substantial amount in the high-speed flow case, where the fringe shift through the visible portion of the boundary layer is only 2 fringe widths. Other random errors occur in the determination of the height of the free-stream boundary and in the wall location. The free-stream boundary is the point where the velocity becomes equal to that of the main stream and, for a fluid with a Prandtl number of 1.0, must be the point where $\rho_n = \rho_\infty$ or where $\frac{\partial S}{\partial y} = 0$. It follows that there might be some difficulty in defining the thickness δ within a small tolerance, especially if small disturbances caused by turbulent eddies in the side-wall boundary layers are superimposed. The situation is further complicated by the unknown but probably uniform error caused by the corner radius, and the actual fluctuation of the position of the free-stream boundary itself.

Wall-location error occurs because of the fact that in the photographs of the test section, with or without flow, the surface of the bottom plate is not sharply defined. A mixture of reflected, refracted, and diffracted light produces various fringe patterns that tend to obscure the plate surface. In order to facilitate a more accurate estimate of the location of this surface, a system of reference wires

0.003 inch in diameter were photographed through the disturbance, along with the interference pattern. With this grid, the magnification of the picture could be determined and the location of the wall plotted on each interferogram.

The measured position of the free-stream boundary is plotted against flow length in figure 6 for the various combinations of free-stream velocity and wall condition. At the shorter flow lengths the random errors of fringe-position measurement are expected to predominate because of the thinness of the layer and lack of large-scale turbulence in either the side-wall or the bottom boundary layers. Since the plots look reasonably smooth in this region it might be guessed that the random measuring errors are small and that the large fluctuations in the free-stream boundary position at the longer flow lengths are due mainly to the turbulent eddies in the boundary layer under study. Random errors in measurement can be minimized statistically; if enough cross sections are averaged together, these errors should tend to disappear. Other measuring errors of a systematic nature caused by the processing of the interferograms (such as magnification error) can be minimized by nondimensionalizing the resulting data.

Errors which do not vary with y in either a random or a uniform manner, however, are not affected by averaging or by nondimensionalization. Refraction is one of these errors. Since present evaluation equations involving refraction correction are cumbersome, one solution might be to establish that in the turbulent boundary layer under study, refraction can be considered negligible.

Refraction has three simultaneous effects on the trajectories of the light rays passing through a cooled boundary layer. These are: (1) an integrating effect due to the fact that the light ray is bent toward the wall and traverses succeeding layers of increasing density, instead of remaining in the original layer as is assumed when refraction is neglected; (2) a distortion effect caused by a vertical displacement of the ray which makes it appear to emerge from the test section at a point different from its assumed emergent height; and (3) a cutoff effect in which a large density gradient causes light rays near the surface to be bent onto the surface of the plate and prevents observation of the portion of the boundary layer very close to the wall.

An analytical investigation of these refraction errors for cooled boundary layers has been reported in reference 9. In this reference, equations are derived and used to compute the paths of light rays through particular steady-flow boundary layers as well as the approximate errors that result from the refraction effects. These calculations, when applied to the test conditions of both the high- and low-speed boundary layers of this report, show refraction to be negligible for the boundary-layer profiles presented. In addition, the measurements

of the light cutoff in the present case were compared with that predicted by the theoretical calculations of reference 9. The calculated values of refraction of reference 9 for these boundary layers were found to be too large by an order of magnitude or more.

A qualitative estimate of the effects of refraction may also be obtained directly from the interference photographs. The effects of refraction act simultaneously, and it will be shown that two of the three effects can be measured directly on the interferograms. It might be reasoned that if two of the three effects can be demonstrated to be infinitesimal, the remaining effect may also be assumed to have small influence on the measured fringe shift.

To measure the distortion effects, the previously mentioned reference wires were attached to the side of the test section on which the light rays enter the fluid. One of these wires was placed so that it crossed the beam of light diagonally, at approximately a 45° angle with the plate surface. With the interferometer camera focused midway across the test section, any distortion would cause a bend to appear in this wire. No appreciable distortion of the wire was noted on any of the pictures involved, except those of the thin boundary layers at the beginning of transition in the high-density flows.

The other measurable effect of refraction was the light cutoff effect. At the shortest flow lengths of the subsonic free stream over a smooth wall, approximately 1/3 of the boundary-layer thickness disappeared. This effect decreased rapidly with flow length, so that at the end of the transition region only 1/20 of the profile was lost from view. For the rest of the flow lengths, the amount of light that disappeared was approximately the same as that cut off at the end of transition. Since the boundary layer grew considerably thicker, at the longest flow lengths less than 1/60 of the density profile was lost. For the supersonic free-stream flow, the light cutoff was not measurable within the accuracy with which it was possible to plot the location of the surface of the plate on the photographs. It appeared to be approximately 1/22 of the boundary-layer thickness at the beginning of transition and much less than that for the rest of the flow lengths investigated. Therefore, except for the profiles taken at the beginning of transition in the case of the low-velocity free stream, the refraction error can be assumed to be small and can be ignored.

Langley Aeronautical Laboratory,
National Advisory Committee for Aeronautics,
Langley Field, Va., January 29, 1958.

REFERENCES

1. Huber, Paul W., and McFarland, Donald R.: Boundary-Layer Growth and Shock Attenuation in a Shock Tube With Roughness. NACA TN 3627, 1956.

2. Stever, H. G., Witmer, E. A., and Herrmann, W.: The Growth of the Boundary Layer Behind a Shock Wave. 50 Jahre Grenzschichtforschung. Friedr. Vieweg & Sohn (Braunschweig), 1955, pp. 272-279.

3. Martin, W. A.: Boundary Layers in Nonstationary Flow. Progress Report on Research Supported by Grants From the Defence Research Board of Canada 1955-1956, Univ. of Toronto, Inst. Aerophysics, pp. 16-17.

4. Bershader, D., and Allport, J.: On the Laminar Boundary Layer Induced by a Travelling Shock Wave. Tech. Rep. II-22 (Contract N6ori-105), Princeton Univ., Dept. Phys., May 1956.

5. Ladenburg, R., and Bershader, Daniel: Interferometry. Physical Measurements in Gas Dynamics and Combustion. Vol. IX of High Speed Aerodynamics and Jet Propulsion, sec. A, ch. 3, R. W. Ladenburg, ed., Princeton Univ. Press, 1954, pp. 47-78.

6. Howes, Walton L., and Buchele, Donald R.: Practical Considerations in Specific Applications of Gas-Flow Interferometry. NACA TN 3507, 1955.

7. Van Driest, E. R.: Turbulent Boundary Layer in Compressible Fluids. Jour. Aero. Sci., vol. 18, no. 3, Mar. 1951, p. 145-160, 216.

8. Mirels, Harold: Laminar Boundary Layer Behind Shock Advancing Into Stationary Fluid. NACA TN 3401, 1955.

9. Kinsler, Martin R.: Influence of Refraction on the Applicability of the Zehnder-Mach Interferometer to Studies of Cooled Boundary Layers. NACA TN 2462, 1951.

TABLE I.- AVERAGE VALUES OF THE TEST CONDITIONS

	Subsonic free stream		Supersonic free stream	
	Smooth wall	Rough wall	Smooth wall	Rough wall
Total number of cross sections evaluated	141	139	488	141
p_2/p_1	2.078	2.061	24.53	24.48
p_1, lb/sq in. abs	14.73	14.82	0.292	0.292
p_2, lb/sq in. abs	30.60	30.54	7.16	7.15
M_s	1.387	1.382	4.552	4.547
M_2	0.497	0.492	1.770	1.769
u_s, ft/sec	1,580	1,569	5,207	5,165
u_2, ft/sec	632	620	4,223	4,189
ρ_2, slugs/cu ft	38.27×10^{-4}	38.54×10^{-4}	2.389×10^{-4}	2.420×10^{-4}
T_2, $^\circ R$	671	665	2,515	2,478
T_1, $^\circ R$	538	535	543	535
T_w/T_2 (assuming $T_w = T_1$)	0.80	0.80	0.22	0.22
Fringe shift to the wall, S_w (assuming $T_w = T_1$ and very thin boundary layer)	21.8	21.6	20.0	19.8
Ratio of unit flow length to unit picture length, $d\xi/dx$	0.67	0.66	4.28	4.27
R per foot of flow	5.35×10^6	5.32×10^6	0.94×10^6	0.96×10^6

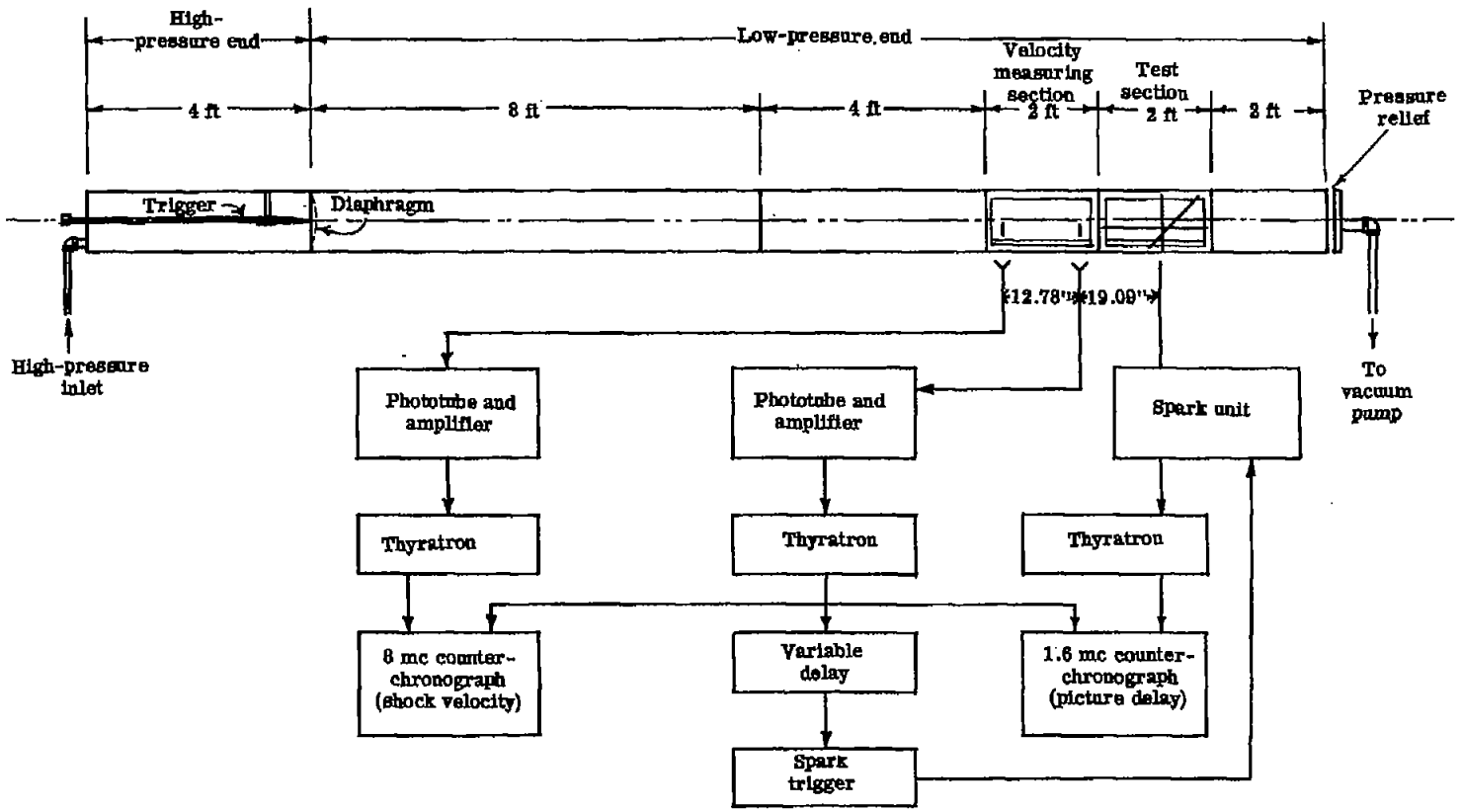

Figure 1.- Schematic arrangement of shock tube and instrumentation.

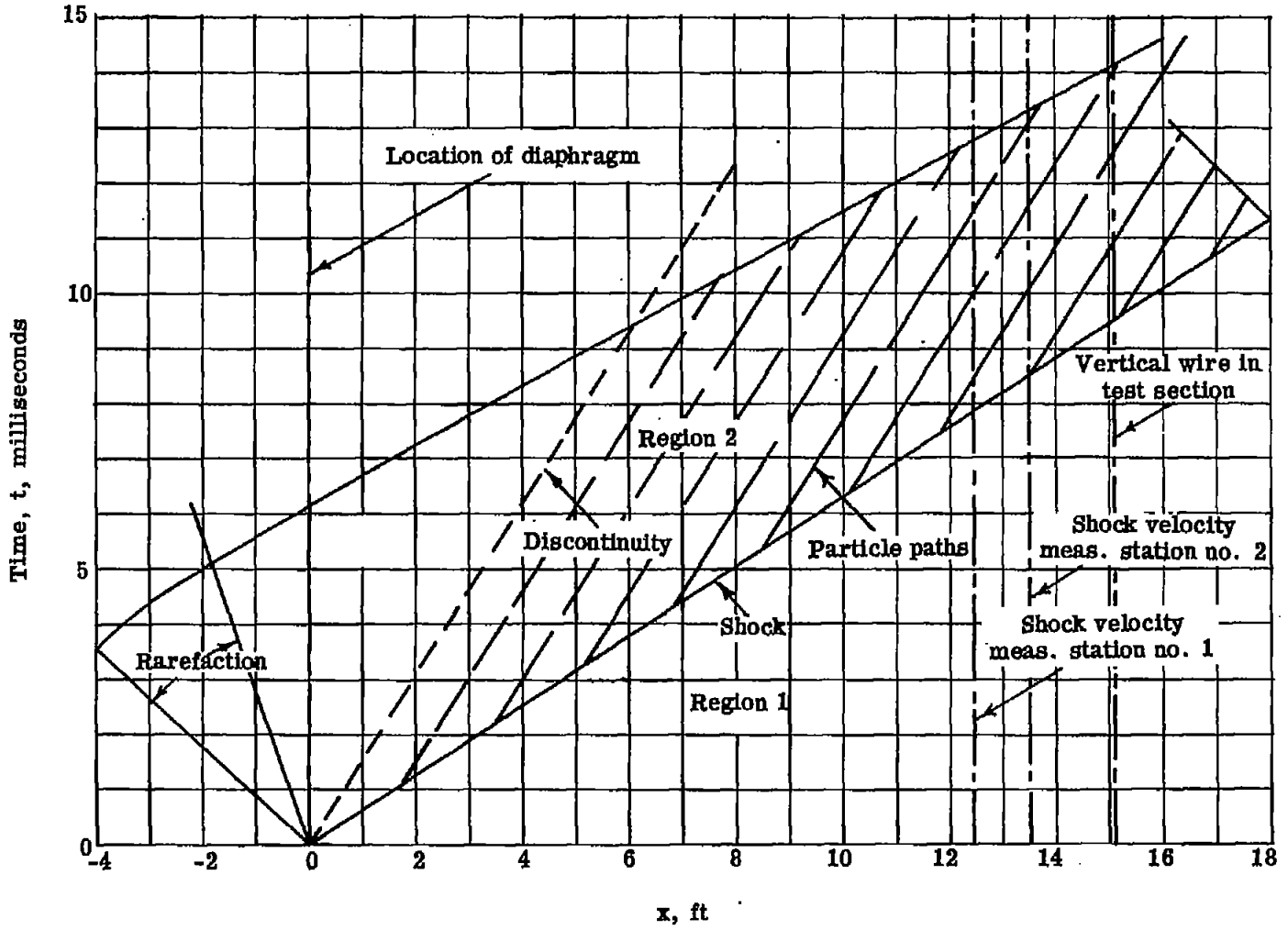

(a) $p_2/p_1 = 2.1$; $M_2 = 0.5$; air/air.

Figure 2.- Distance-time plot of shock-tube flow.

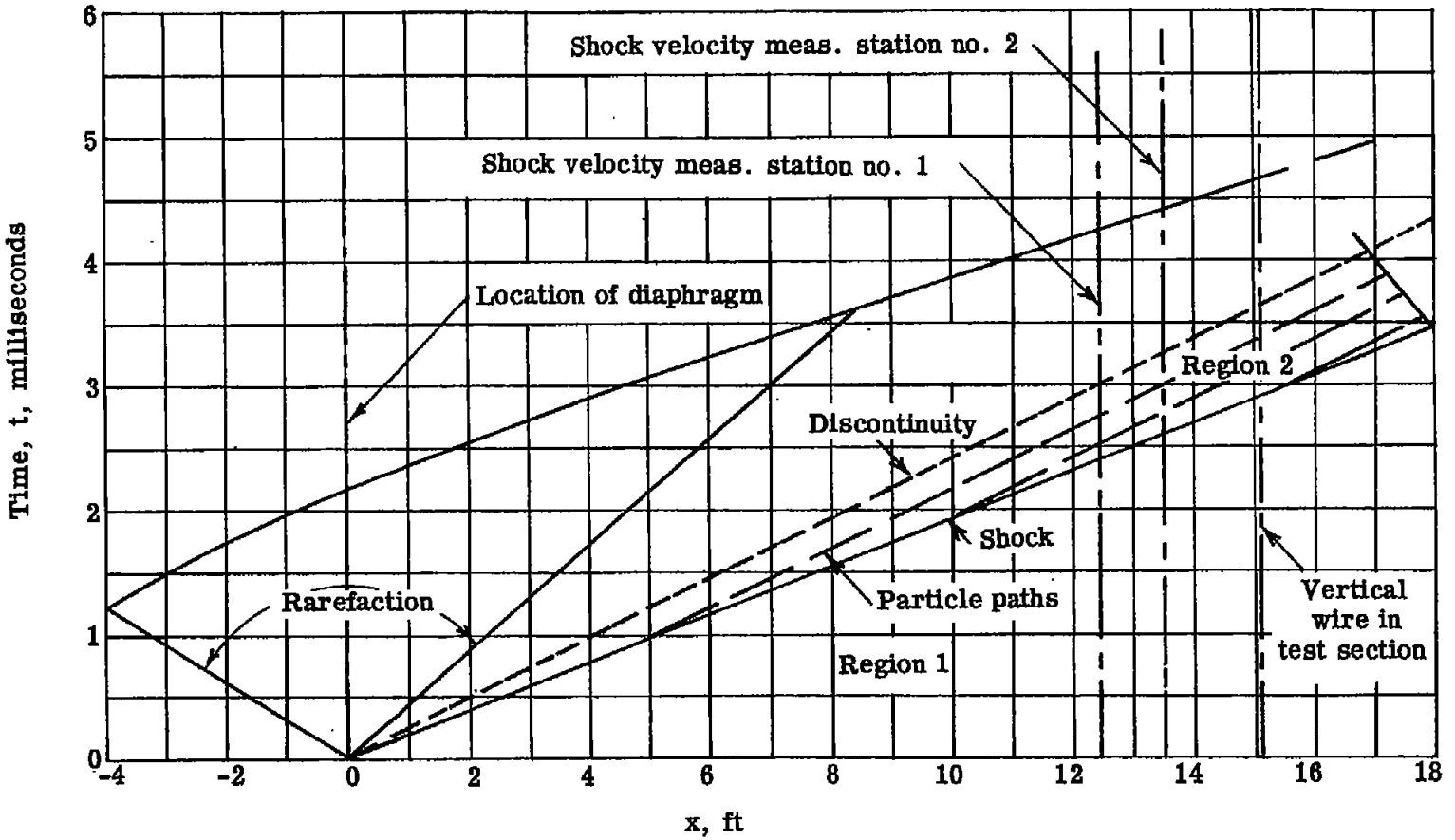

(b) $p_2/p_1 = 24.5$; $M_2 = 1.77$; helium/air.

Figure 2.- Concluded.

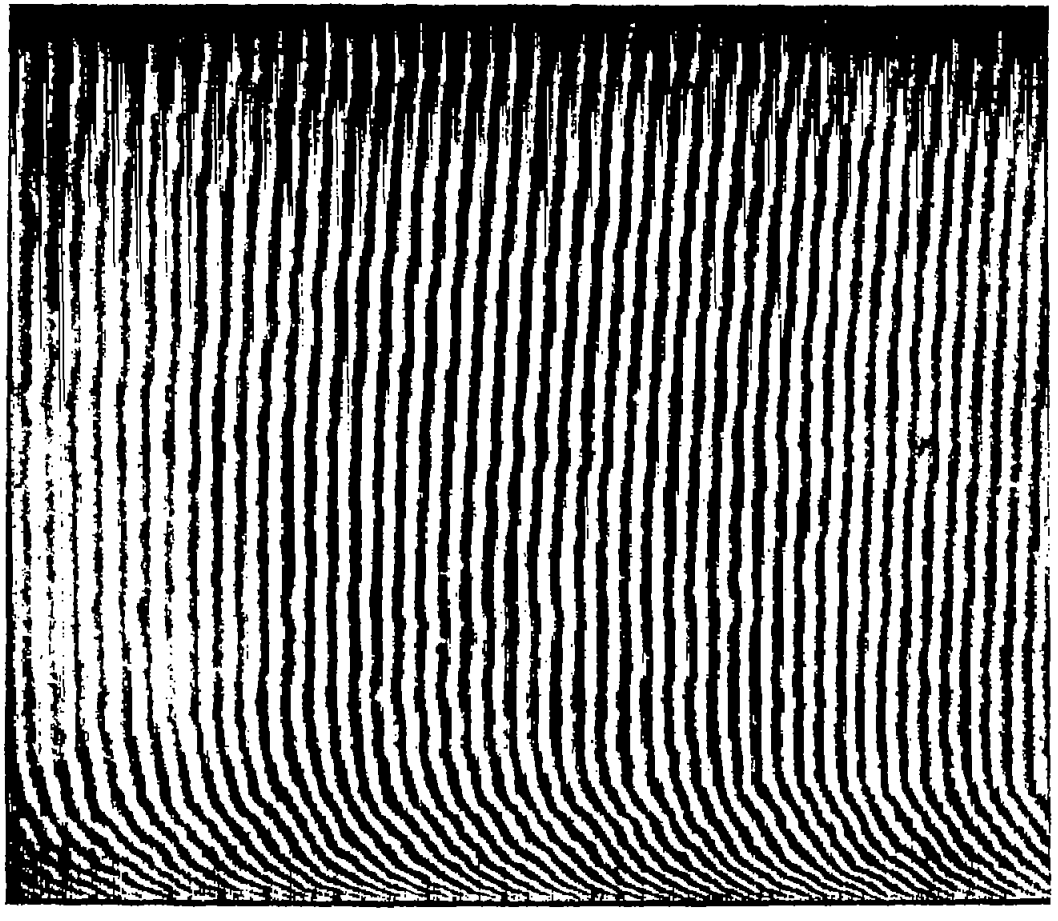

(a) M = 0.50; ξ = 4.16 to 4.33 feet.

Figure 3.- Typical interferograms of the boundary-layer growth on a smooth wall in a shock tube.

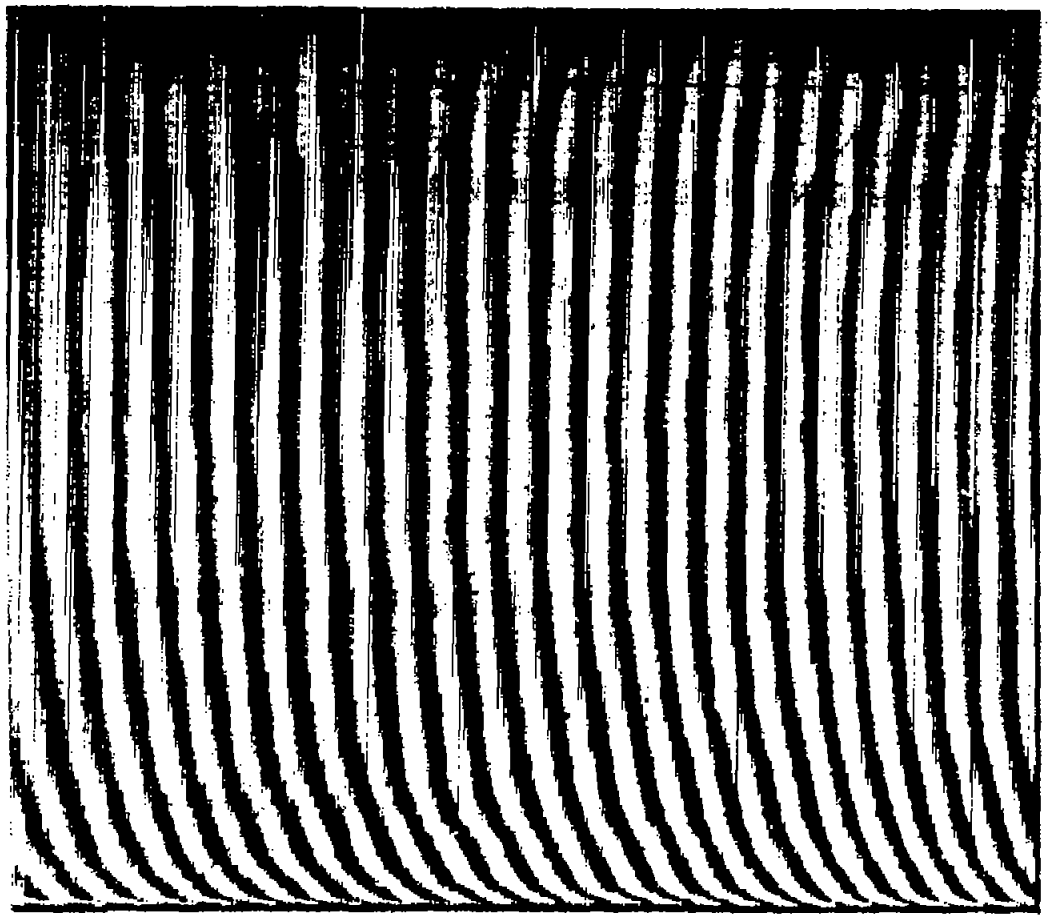

(b) M = 1.77; ξ = 13.5 to 14.6 feet.

Figure 3.- Concluded.

(a) M = 0.50; ξ = 0 to 0.65 feet. L-58-163

Figure 4.- Schlieren photographs of the region of flow immediately behind the advancing shock wave. Movement of shock wave is from left to right. Smooth wall.

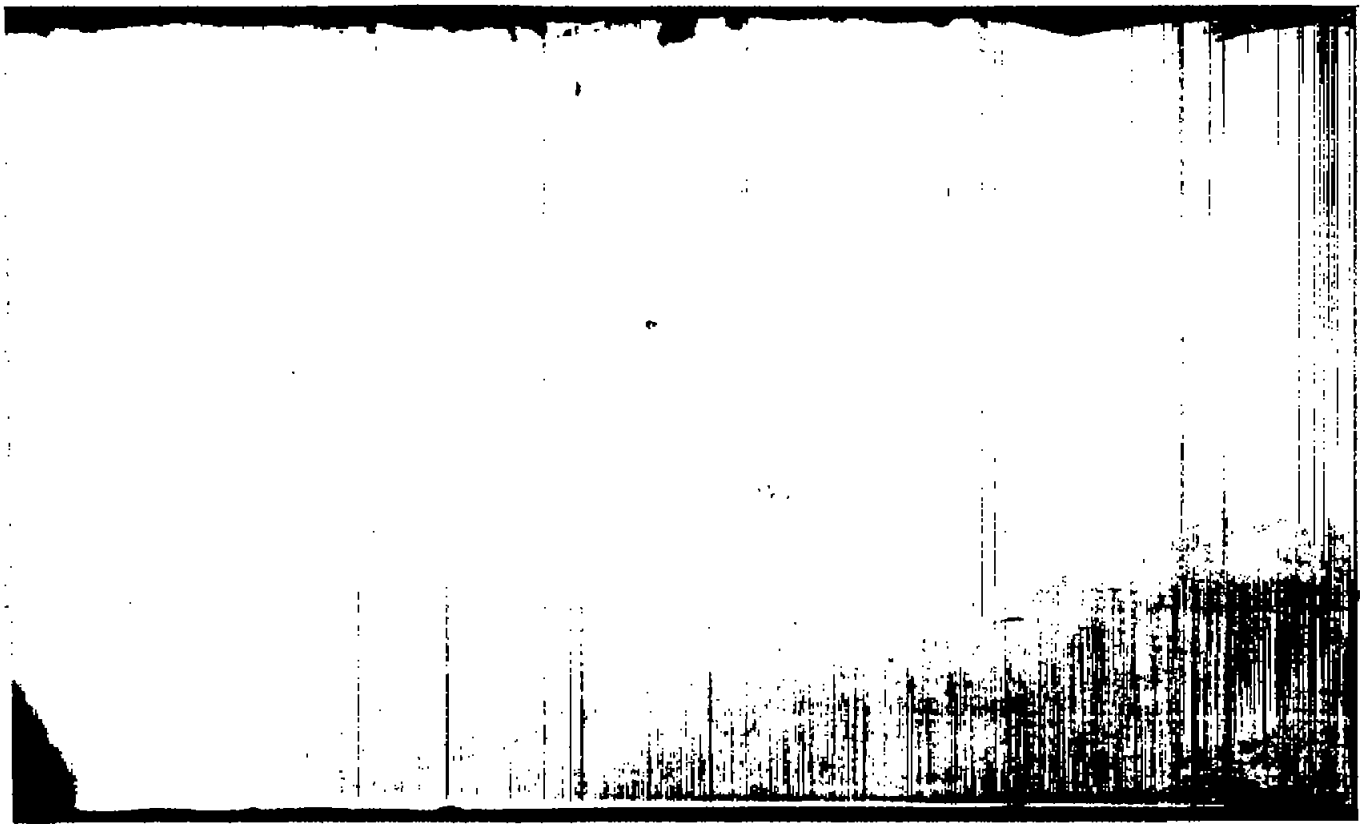

(b) M = 1.77; ξ = 0 to 3.8 feet. L-58-164

Figure 4.- Concluded.

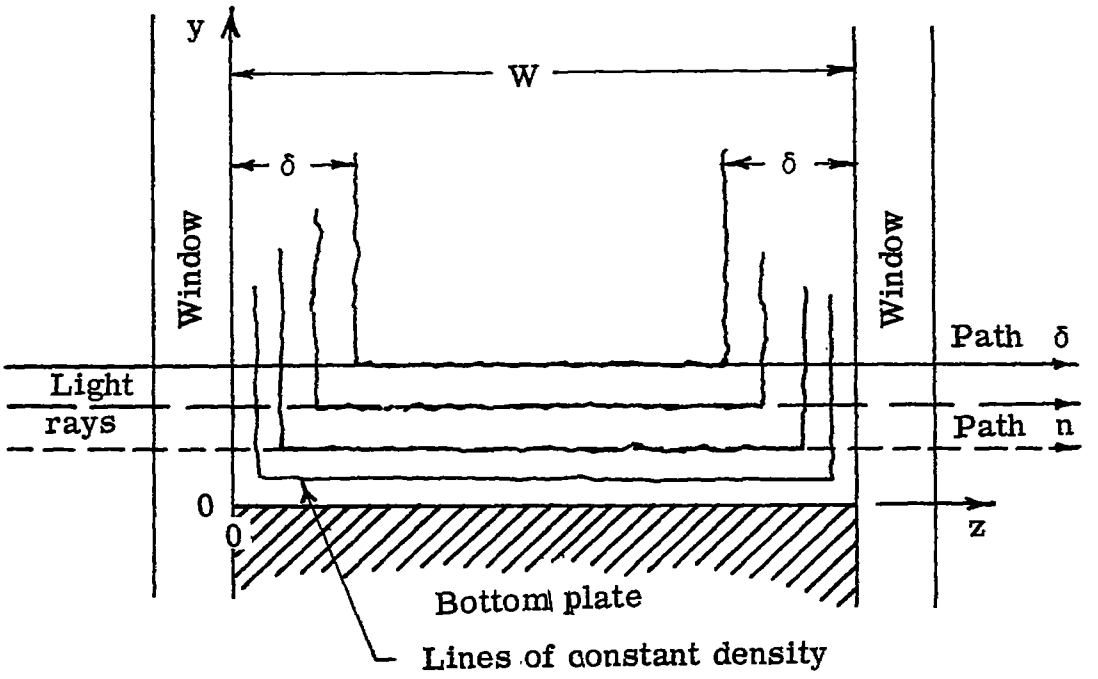

(a) Cross section of channel showing the paths of light rays.

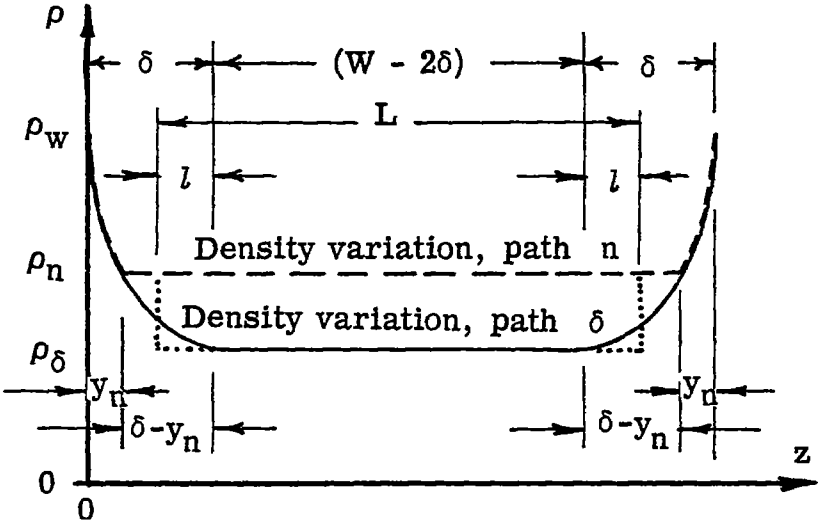

(b) Density variation experienced by the light rays.

Figure 5.- Schematic diagram of the boundary-layer corner effect occurring at the juncture of the shock-tube walls and bottom plate.

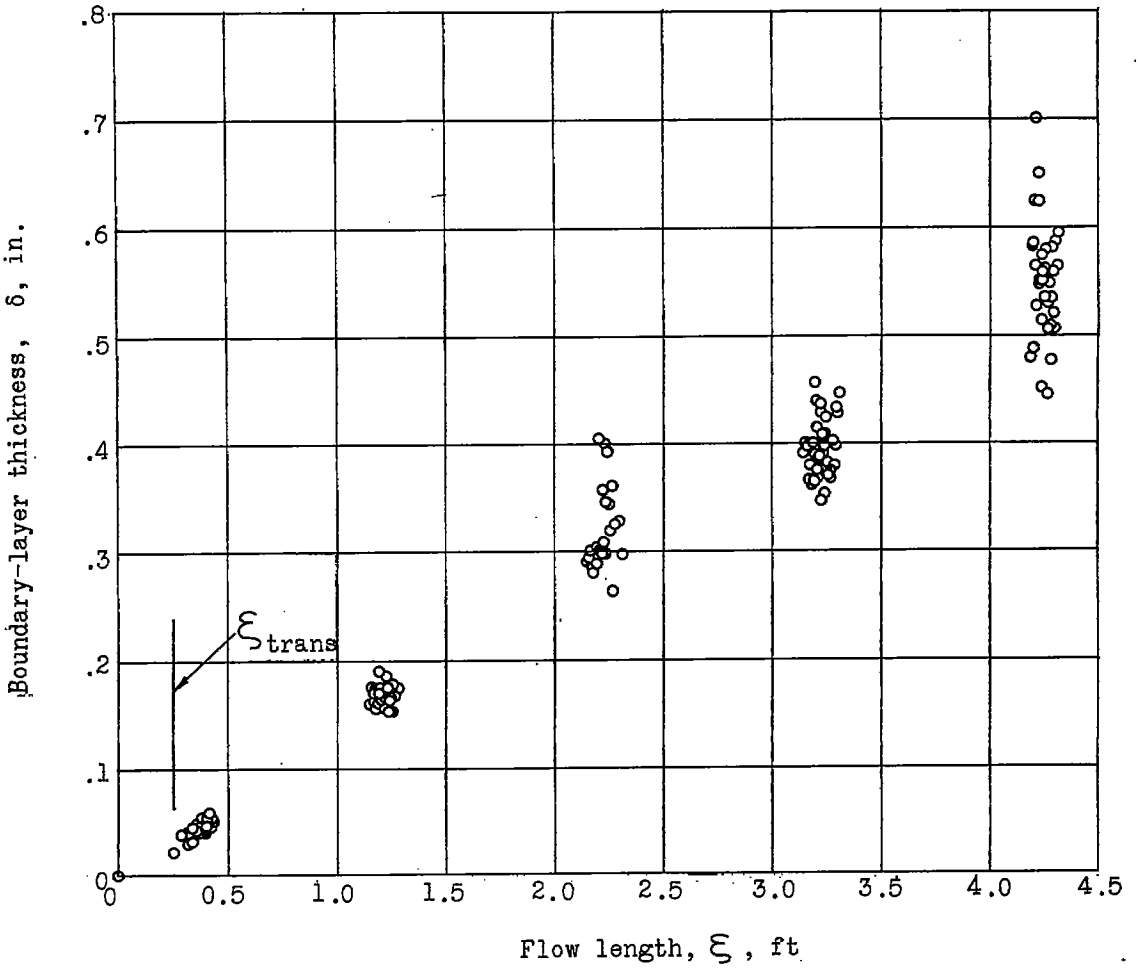

(a) M = 0.50; smooth wall.

Figure 6.- Variation of boundary-layer thickness with flow length.

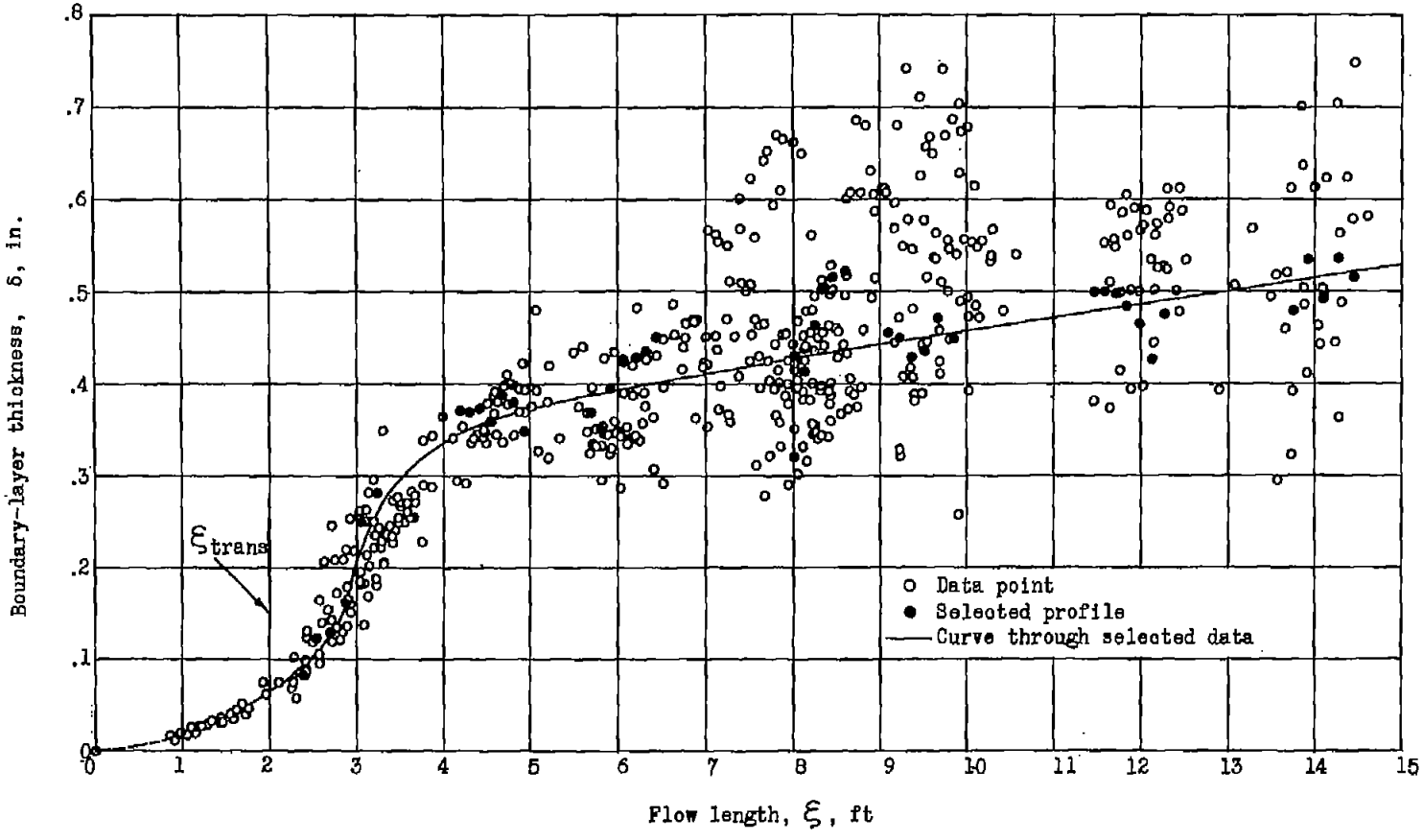

(b) M = 1.77; smooth wall.

Figure 6.- Continued.

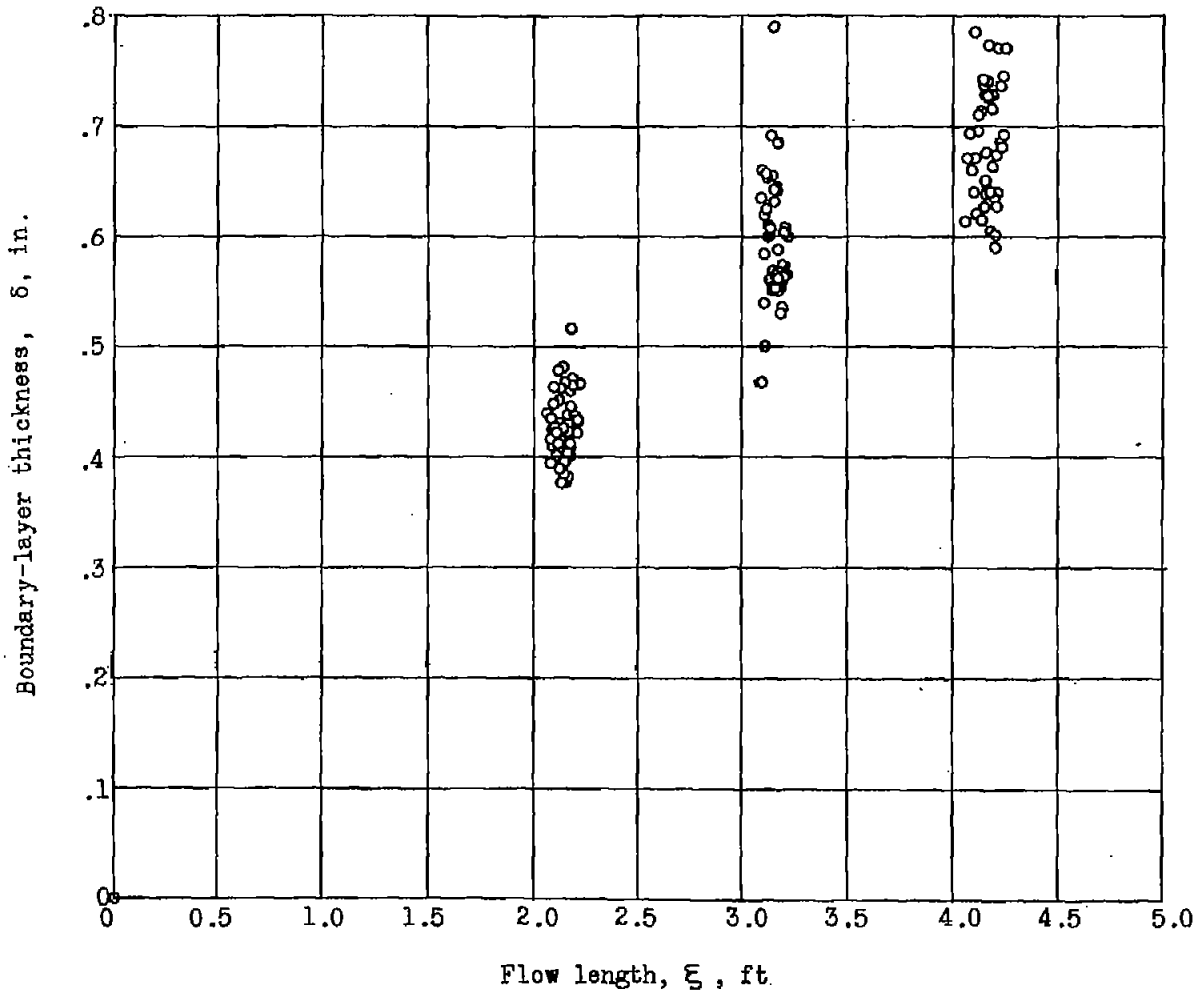

(c) M = 0.49; rough wall.

Figure 6.- Continued.

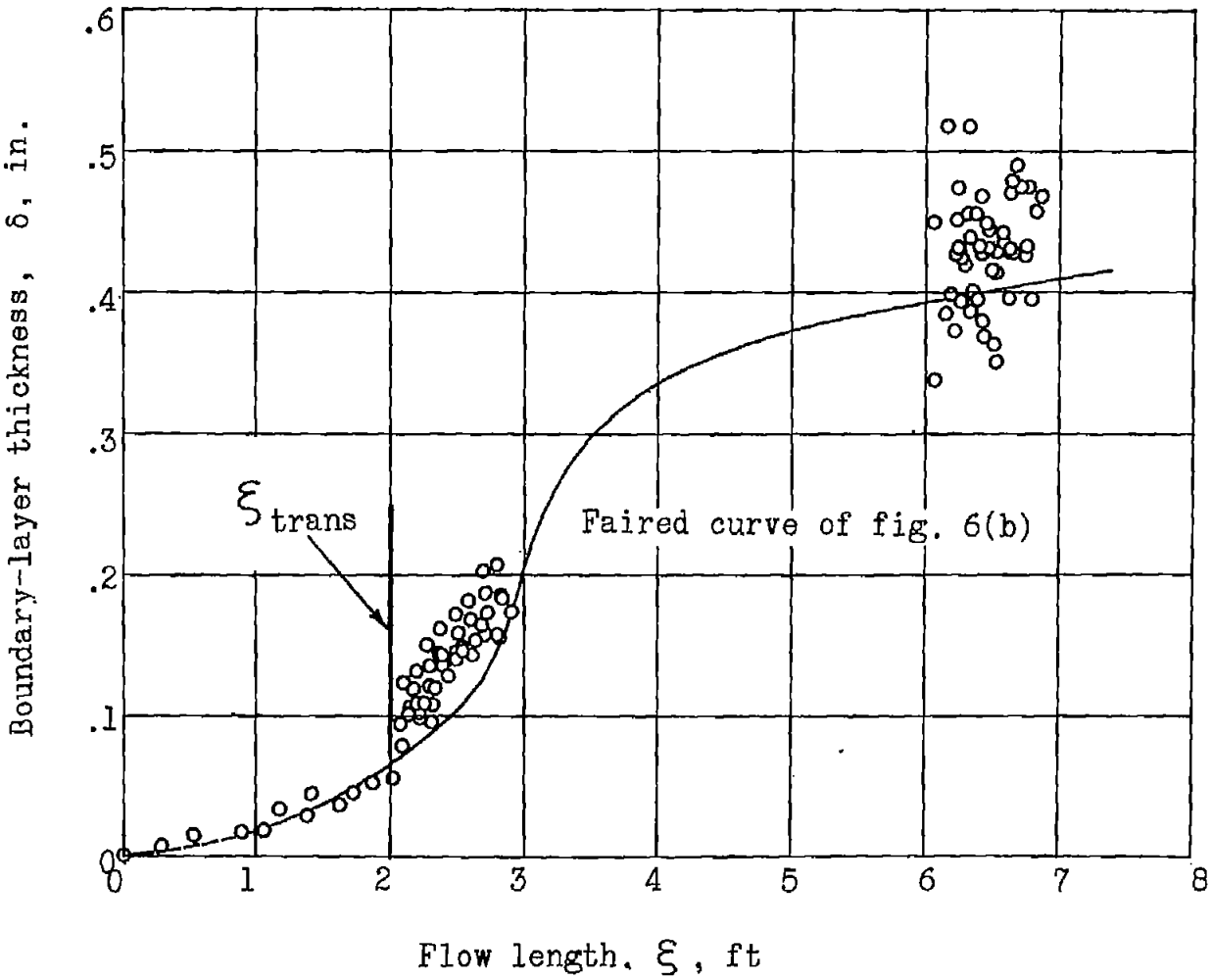

(d) M = 1.77; rough wall.

Figure 6.- Concluded.

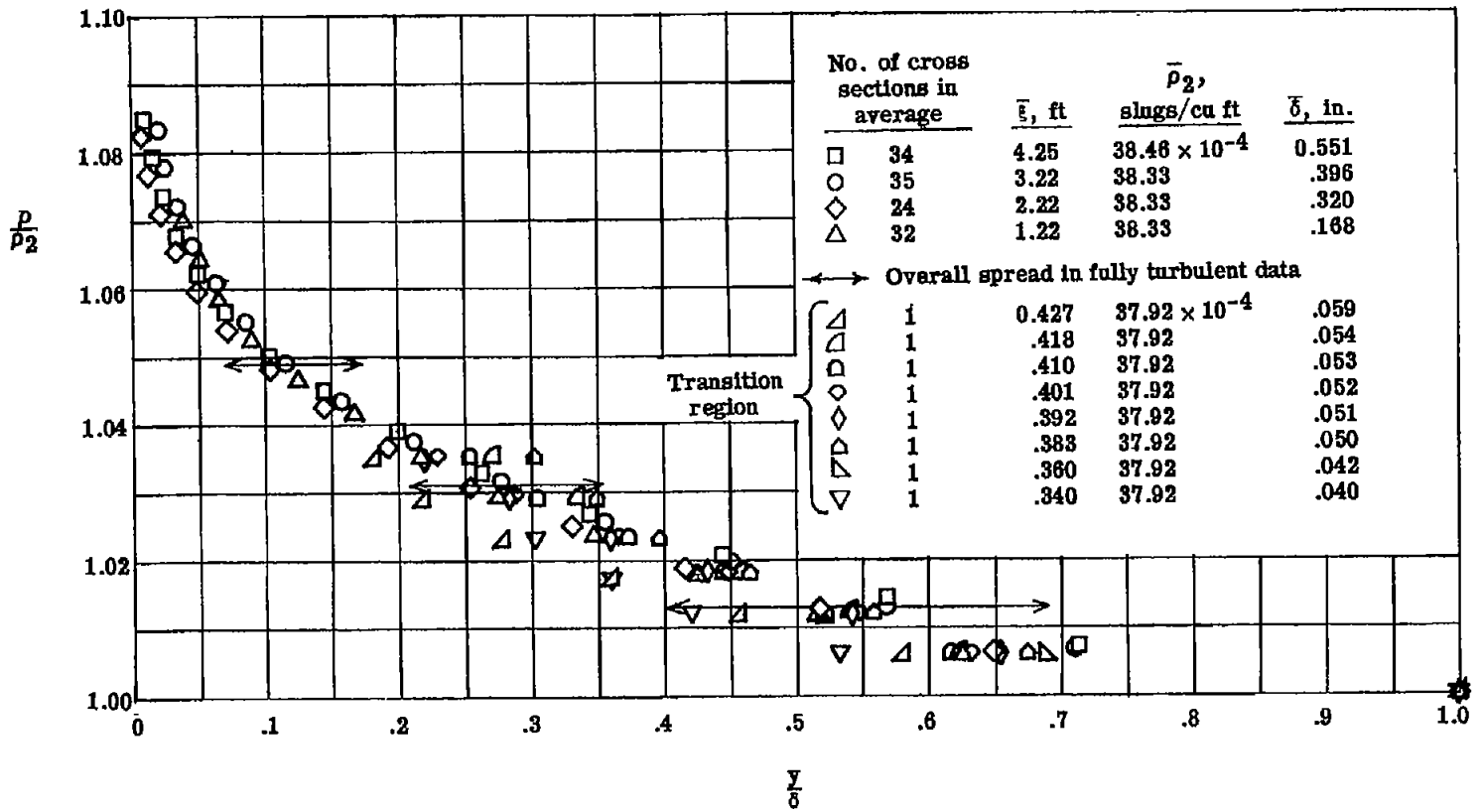

(a) Density variation.

Figure 7.- Profiles through the boundary layer on a smooth wall. $M_2 = 0.50$; $T_w/T_2 = 0.80$; Reynolds number per foot, 5.35×10^6.

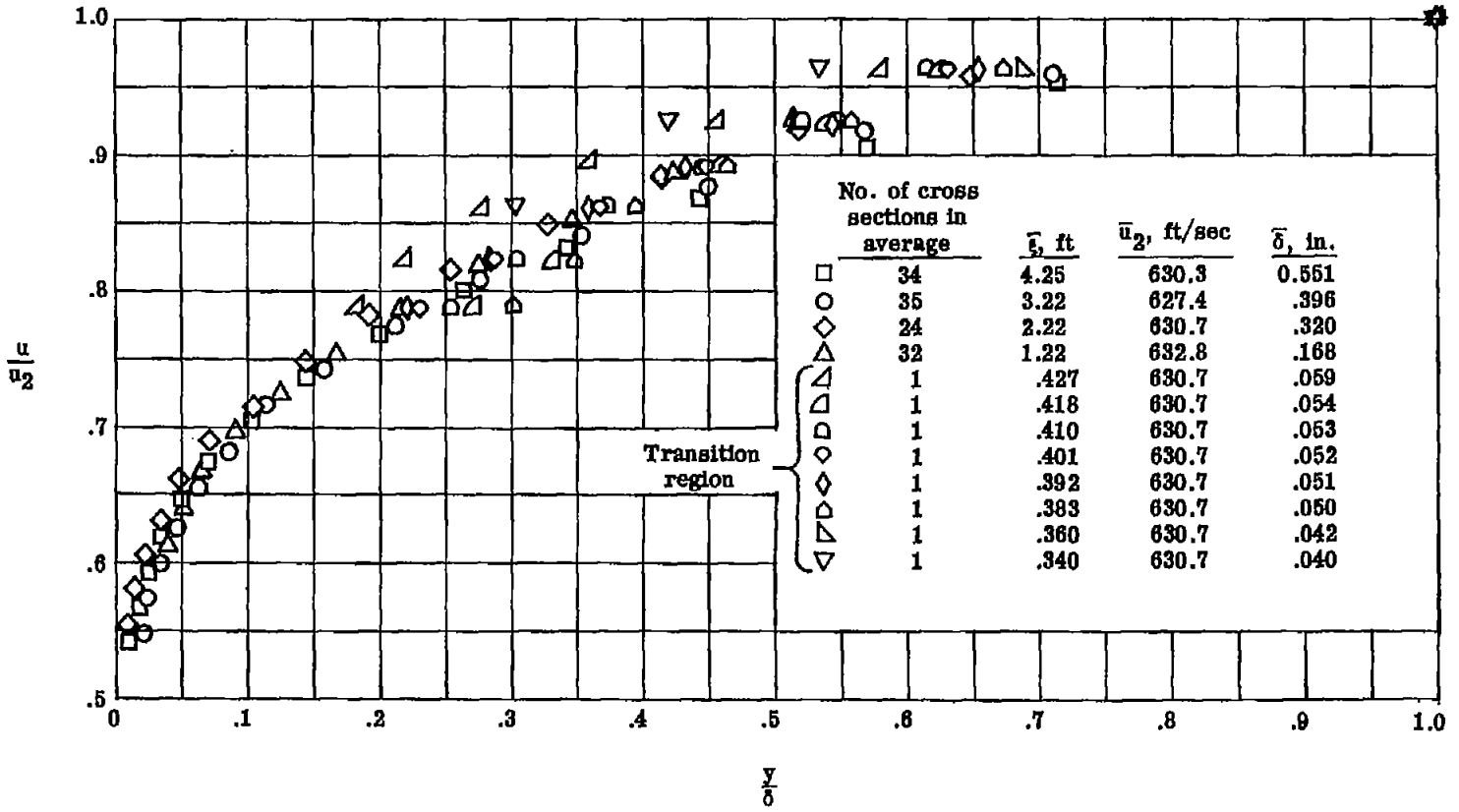

No. of cross sections in average	$\bar{s}$, ft	$\bar{u}_2$, ft/sec	$\bar{\delta}$, in.
34	4.25	630.3	0.551
35	3.22	627.4	.396
24	2.22	630.7	.320
32	1.22	632.8	.168
1	.427	630.7	.059
1	.418	630.7	.054
1	.410	630.7	.053
1	.401	630.7	.052
1	.392	630.7	.051
1	.383	630.7	.050
1	.360	630.7	.042
1	.340	630.7	.040

(b) Velocity distribution.

Figure 7.- Concluded.

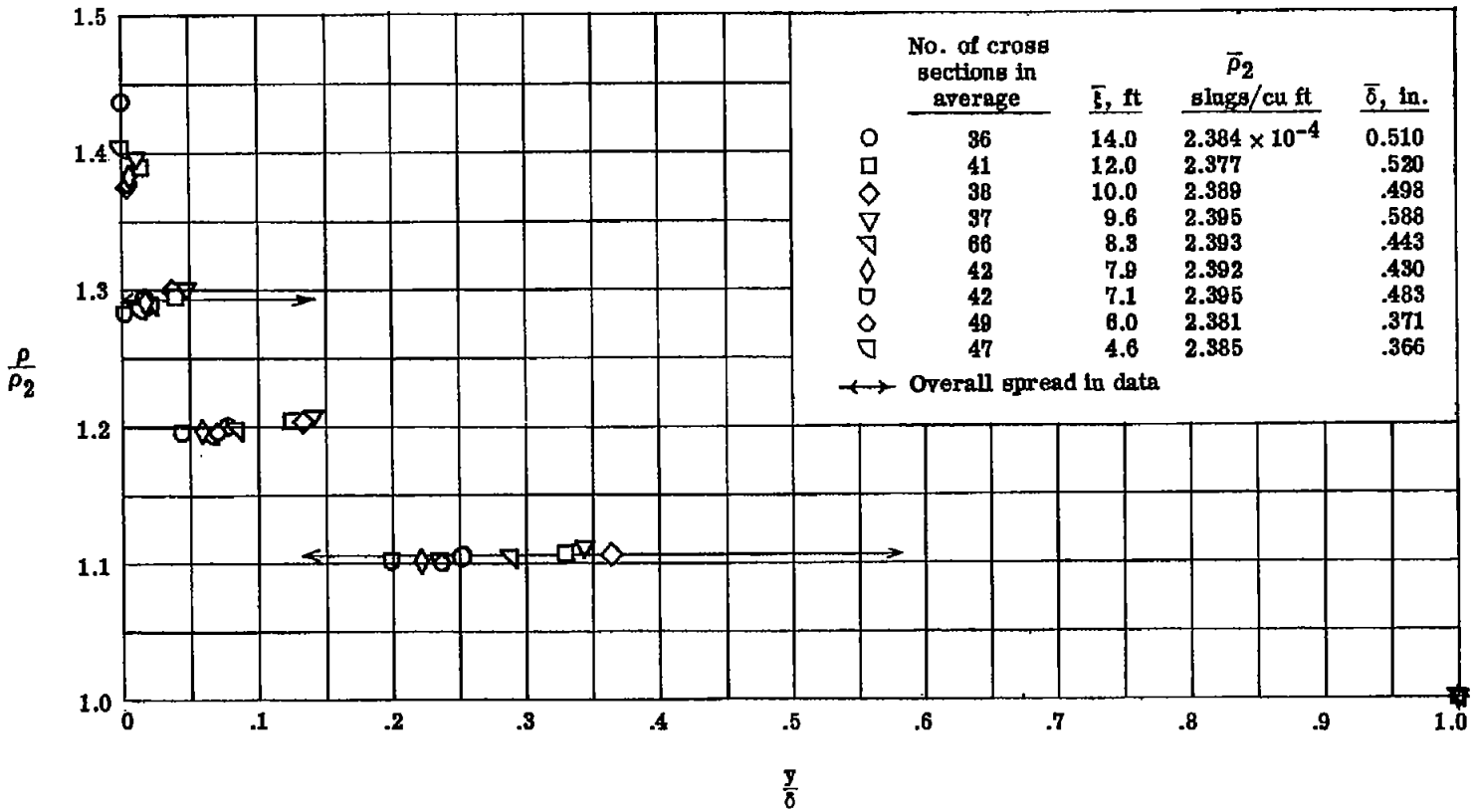

(a) Density variation.

Figure 8.- Average profiles through the turbulent boundary layer on a smooth wall. $M_2 = 1.77$; $T_w/T_2 = 0.22$; Reynolds number per foor, 0.94×10^6.

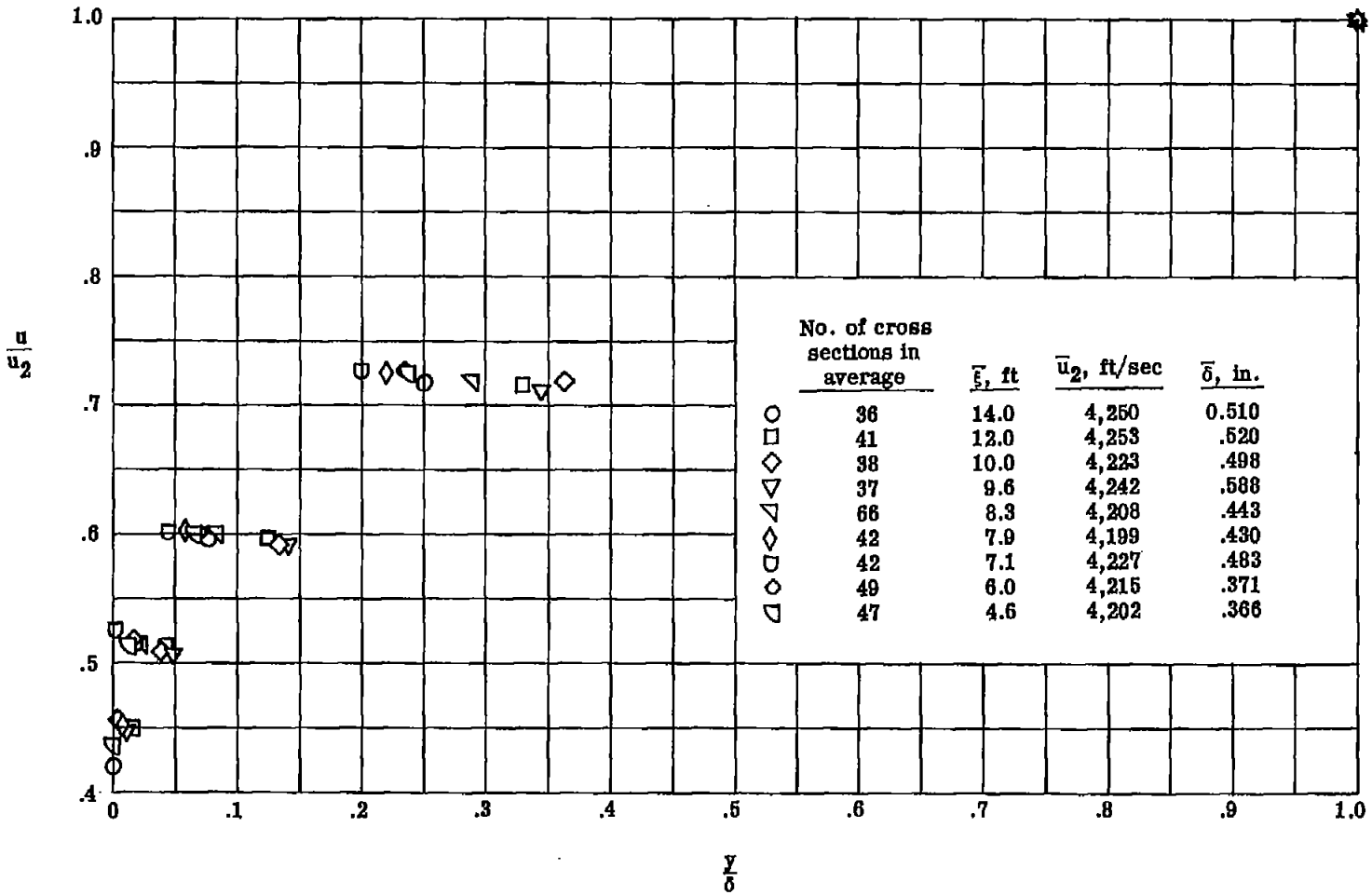

(b) Velocity variation.

Figure 8.- Concluded.

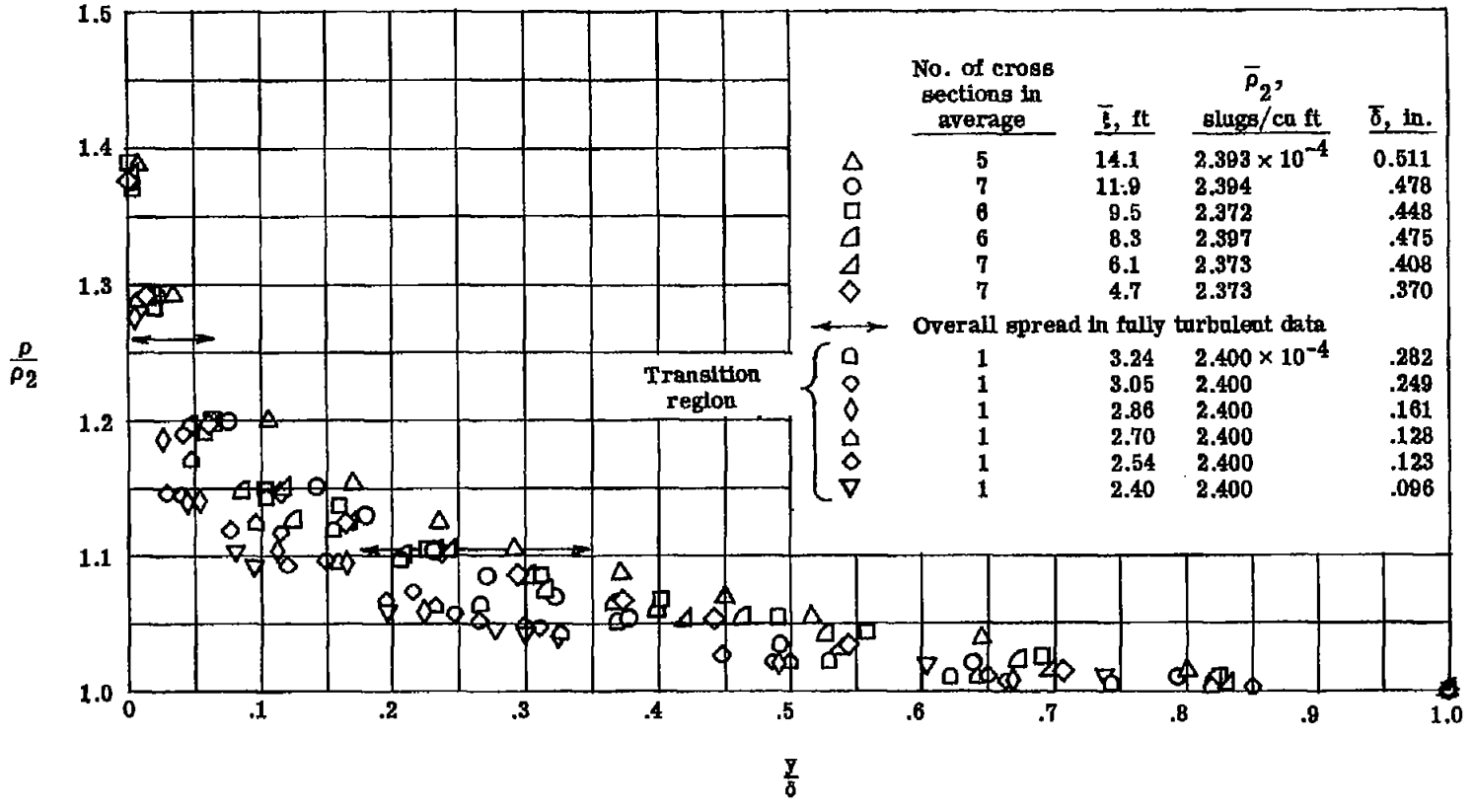

(a) Density variation.

Figure 9.- Selected profiles through the boundary layer on a smooth wall. $M_2 = 1.77$; $T_w T_2 = 0.22$; Reynolds number per foot, 0.94×10^6.

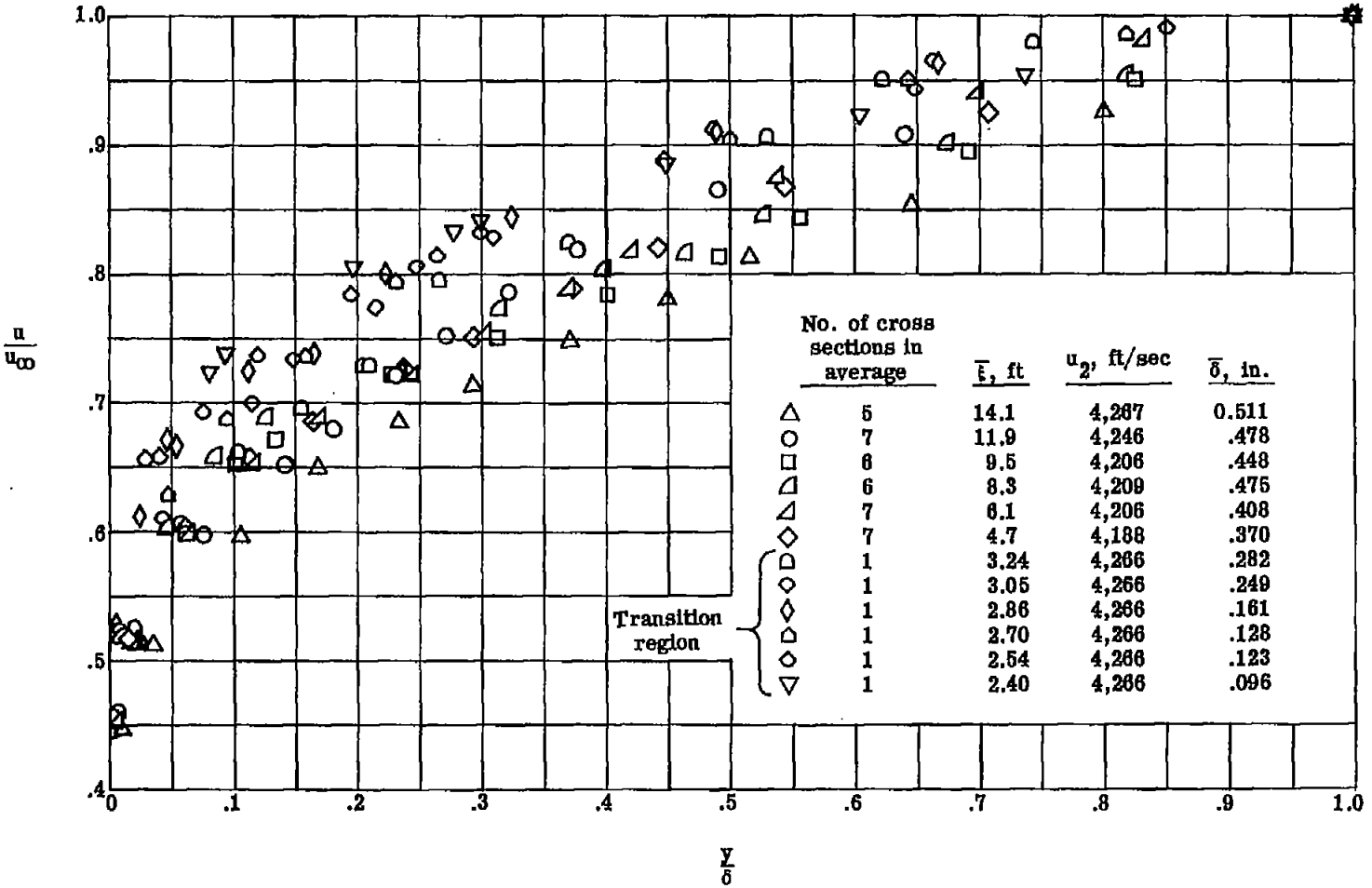

(b) Velocity variation.

Figure 9.- Concluded.

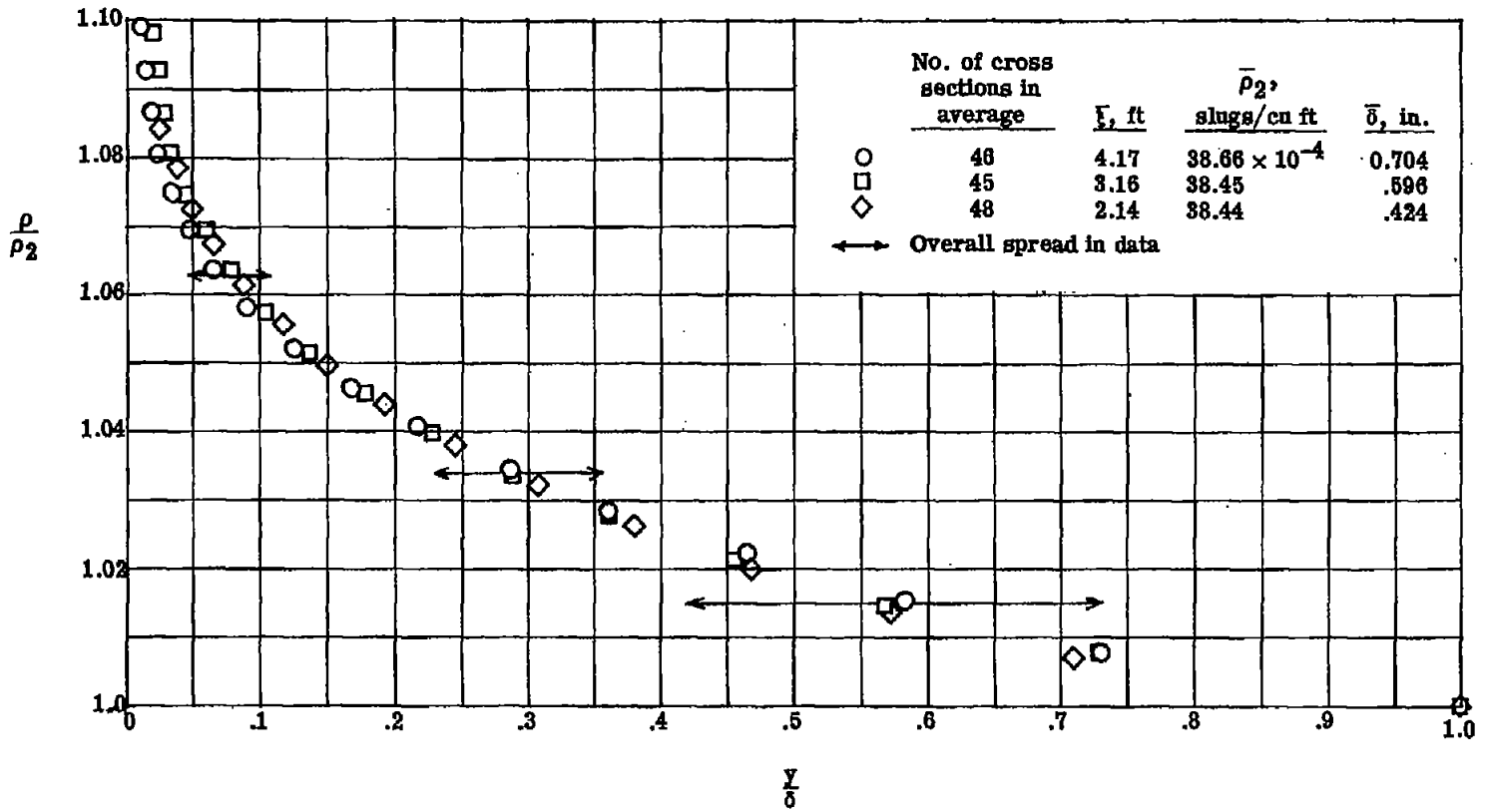

(a) Density variation.

Figure 10.- Average profiles through the turbulent boundary layer on a rough wall. $M = 0.49$; $T_w/T_2 = 0.80$; Reynolds number per foot, 5.32×10^6.

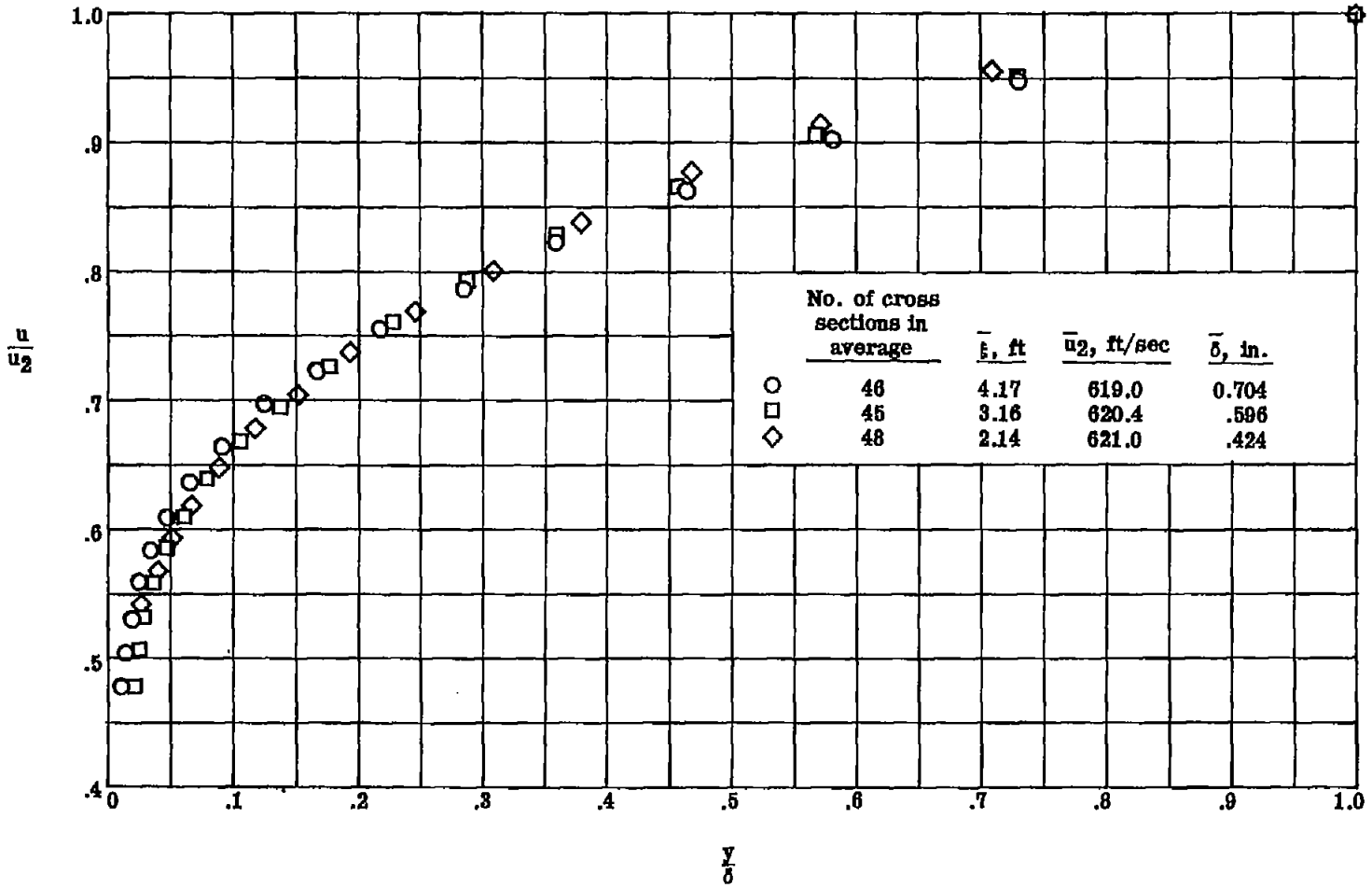

(b) Velocity variation.

Figure 10.- Concluded.

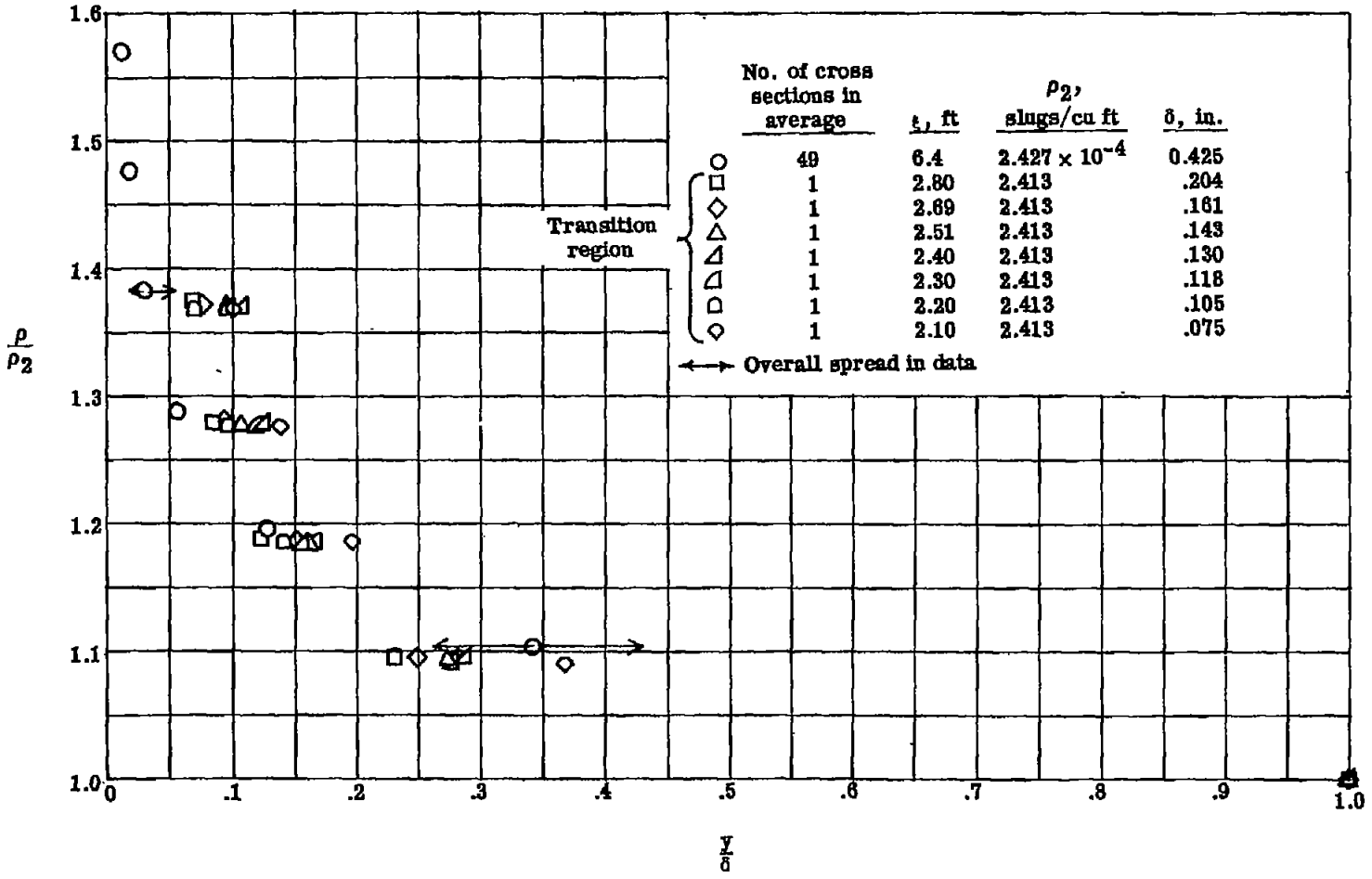

No. of cross sections in average	t, ft	ρ_2, slugs/cu ft	δ, in.
49	6.4	2.427×10^{-4}	0.425
1	2.80	2.413	.204
1	2.69	2.413	.161
1	2.51	2.413	.143
1	2.40	2.413	.130
1	2.30	2.413	.118
1	2.20	2.413	.105
1	2.10	2.413	.075

(a) Density variation.

Figure 11.- Profiles through the boundary layer on a rough wall. $M_2 = 1.77$; $T_w/T_2 = 0.22$; Reynolds number per foot, 0.96×10^6.

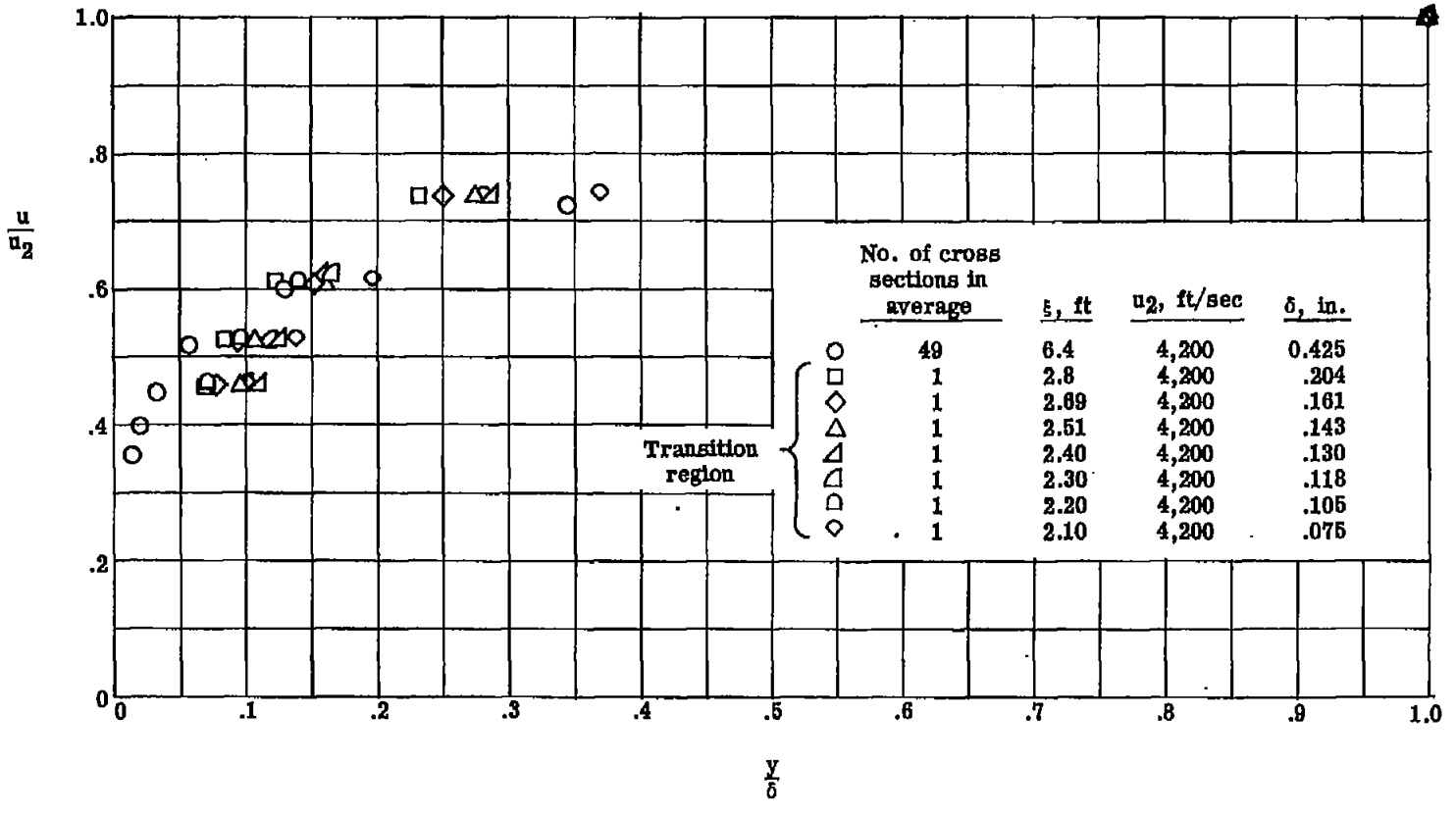

(b) Velocity variation.

Figure 11.- Concluded.

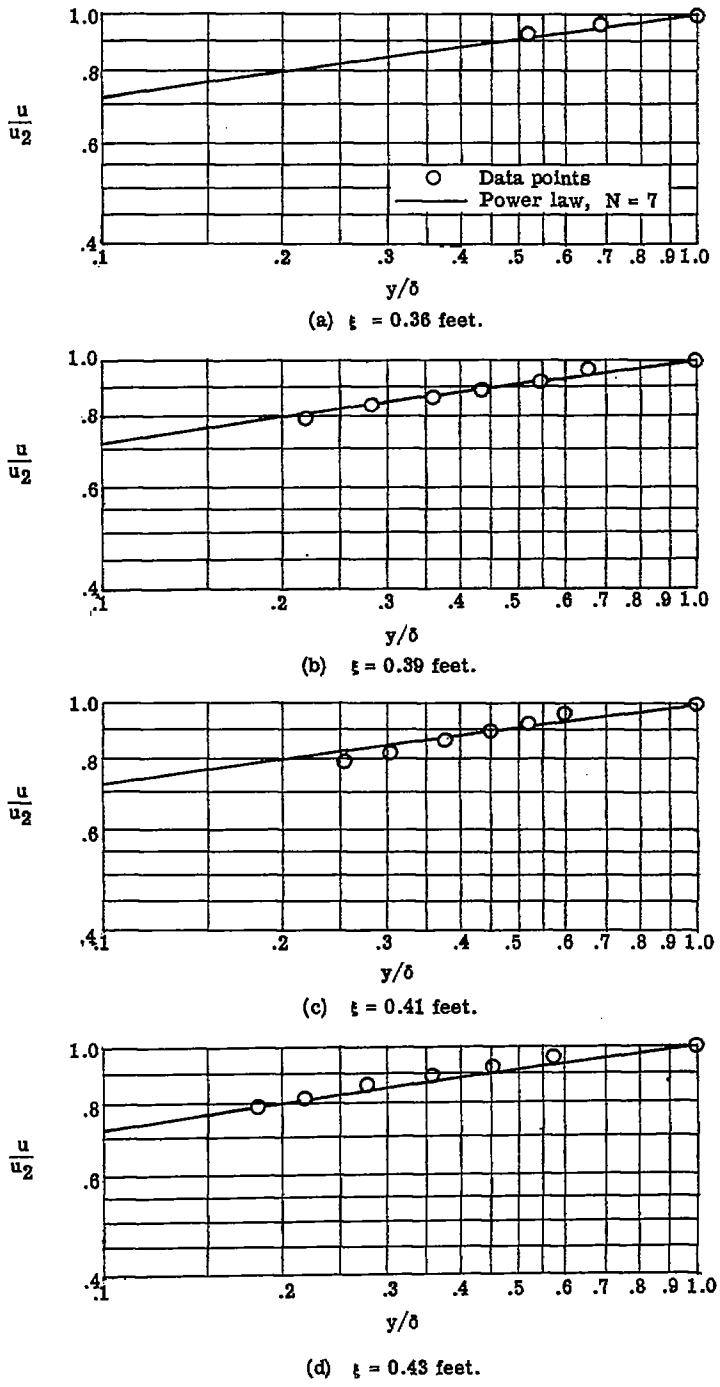

Figure 12.- Velocity profiles through the transition region of the smooth-wall boundary layer at $M_2 = 0.50$ as compared with the one-seventh power law.

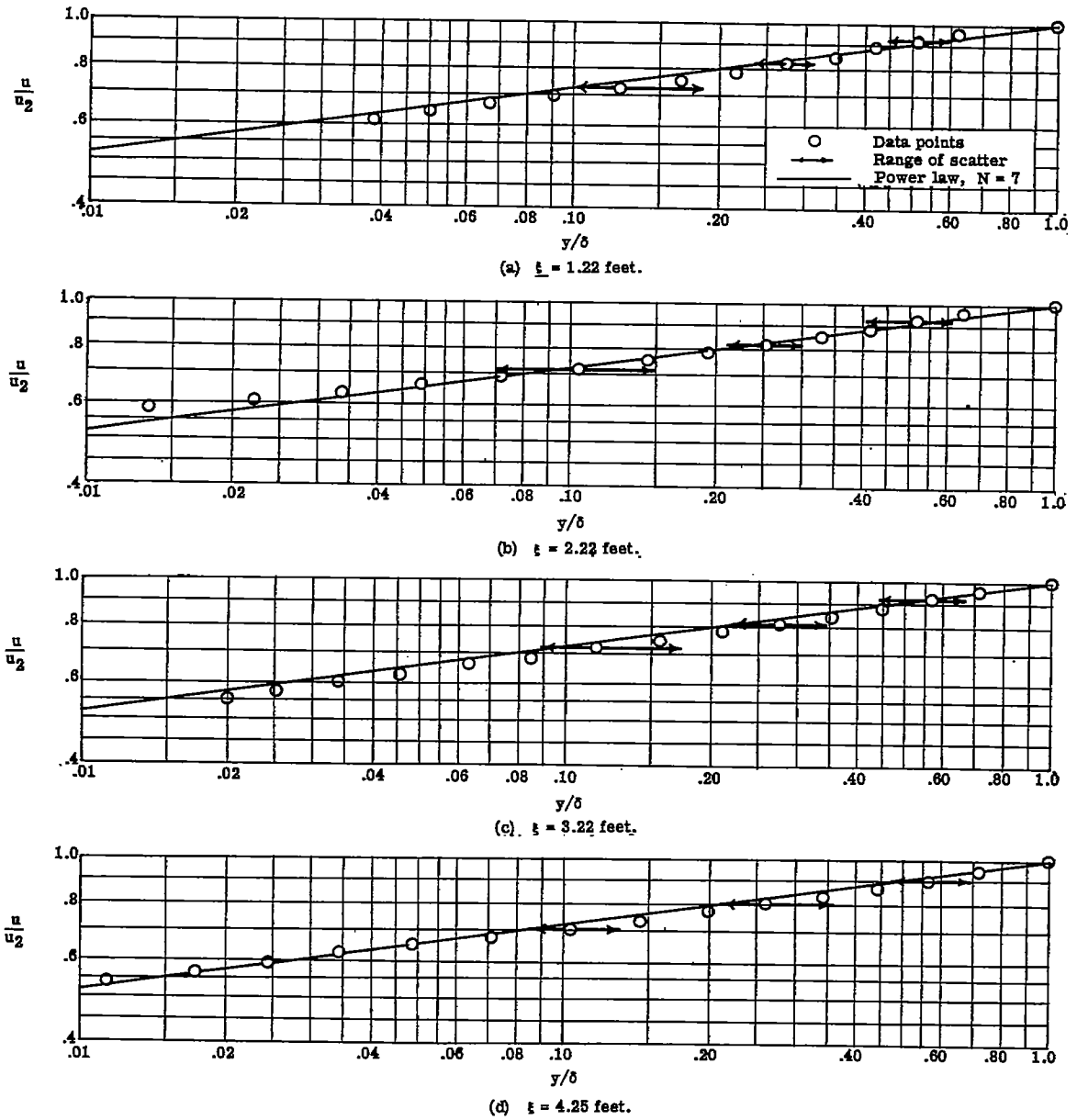

Figure 13.- Average velocity profiles through the smooth-wall turbulent boundary layer for $M_2 = 0.50$ as compared with the one-seventh power law.

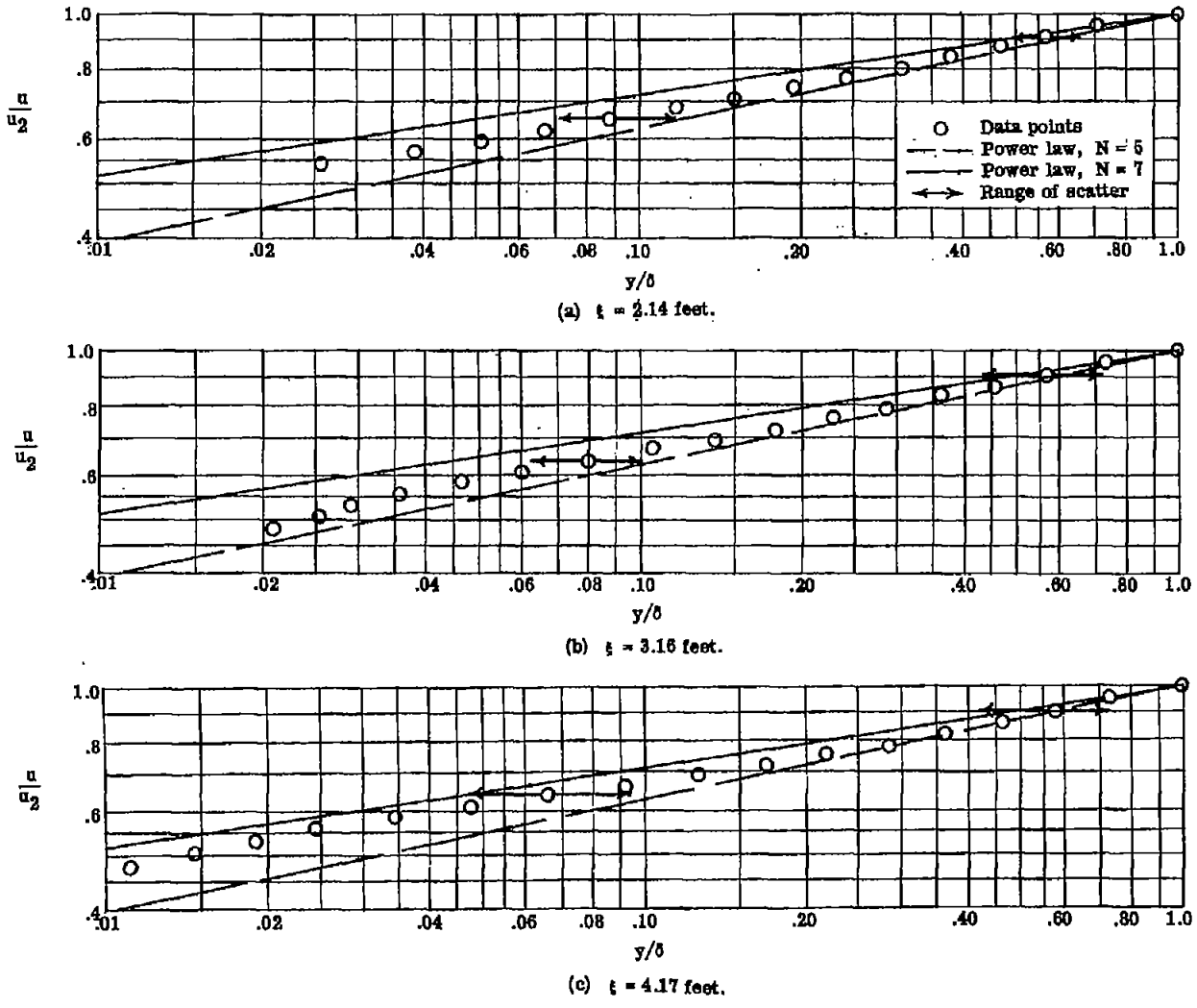

Figure 14.- Average velocity profiles through the turbulent boundary layer on a rough wall for $M_2 = 0.49$ as compared with the one-seventh and one-fifth power laws.

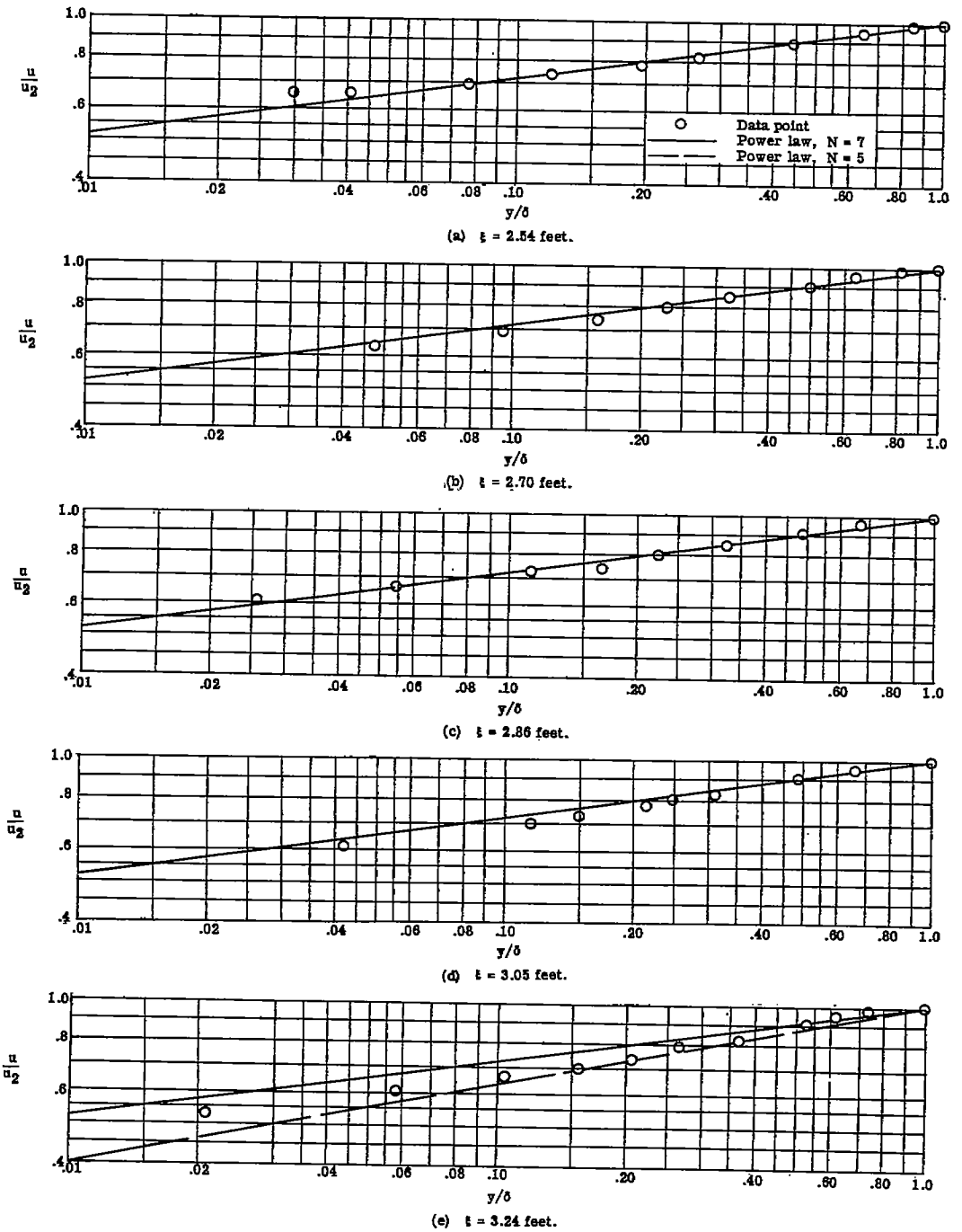

(a) t = 2.54 feet.

(b) t = 2.70 feet.

(c) t = 2.86 feet.

(d) t = 3.05 feet.

(e) t = 3.24 feet.

Figure 15.- Velocity profiles through the transition region of the smooth-wall boundary layer for $M_2 = 1.77$ as compared with the one-seventh and one-fifth power laws.

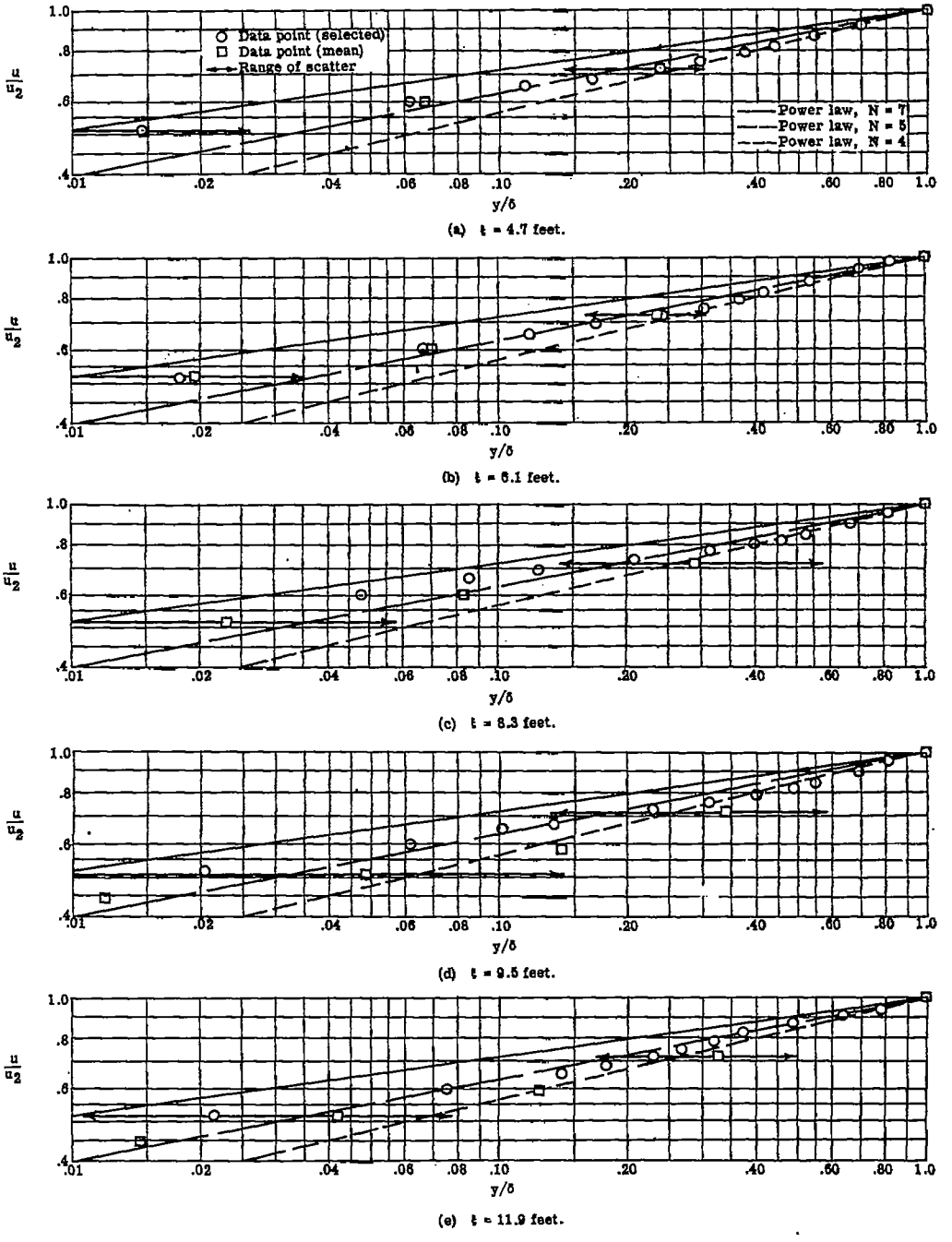

Figure 16.- Velocity profiles through the turbulent smooth-wall boundary layer for $M_2 = 1.77$ as compared with the one-seventh, one-fifth, and one-fourth power laws.

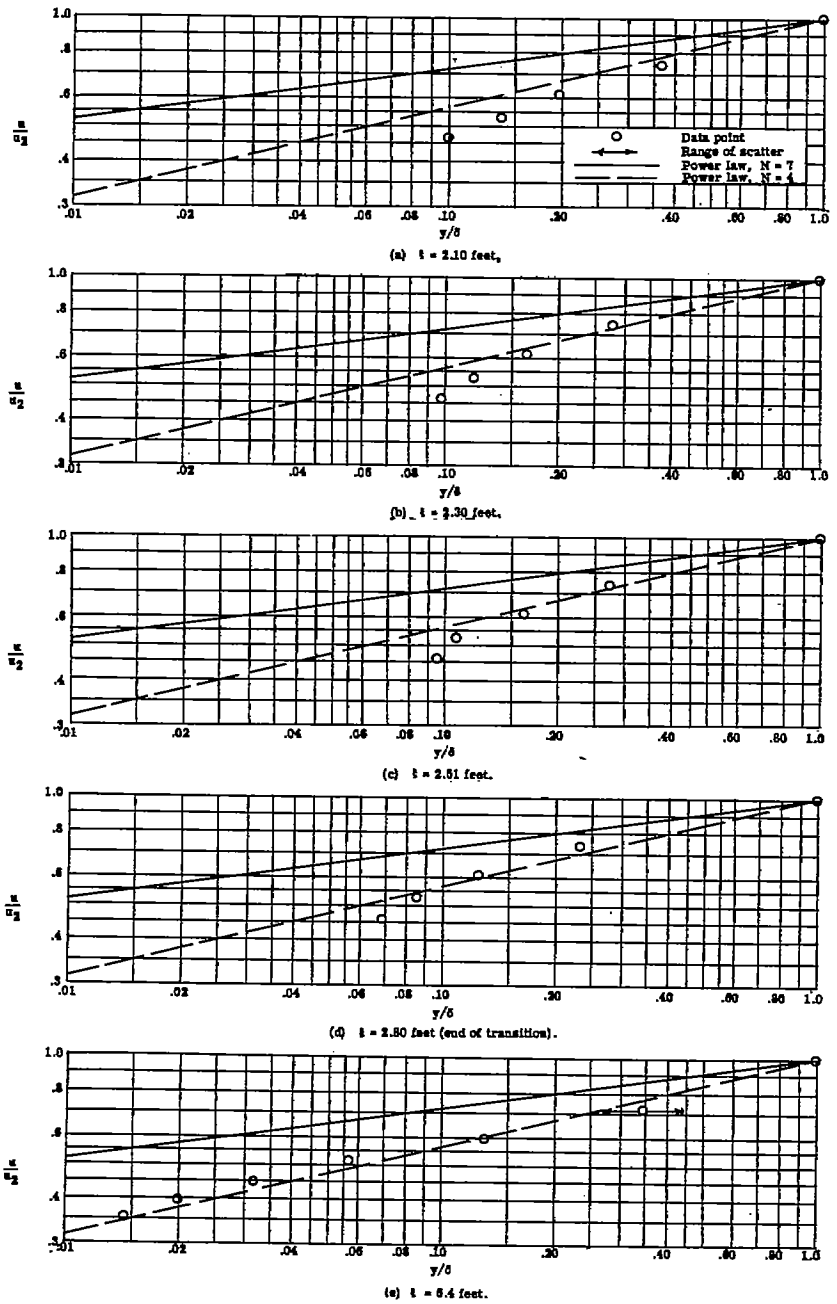

Figure 17.- Velocity profiles through the transition region and an average profile downstream of the transition region for a rough-wall boundary layer at $M_2 = 1.77$ as compared with the one-seventh and one-fourth power laws.

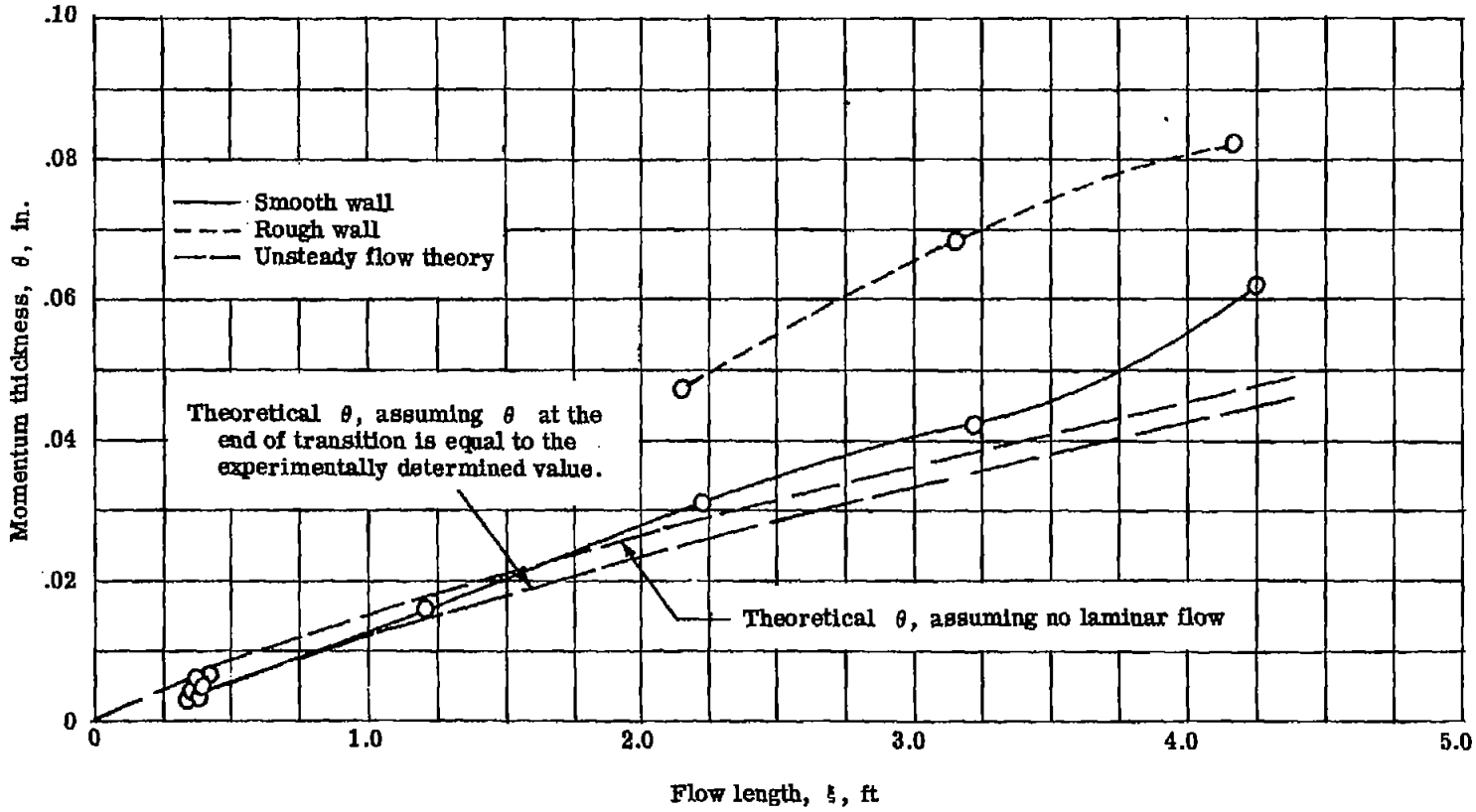

(a) Momentum thickness θ.

Figure 18.- Variation of various average flow parameters with free-stream flow length for $M_2 = 0.50$ (smooth wall) and $M = 0.49$ (rough wall).

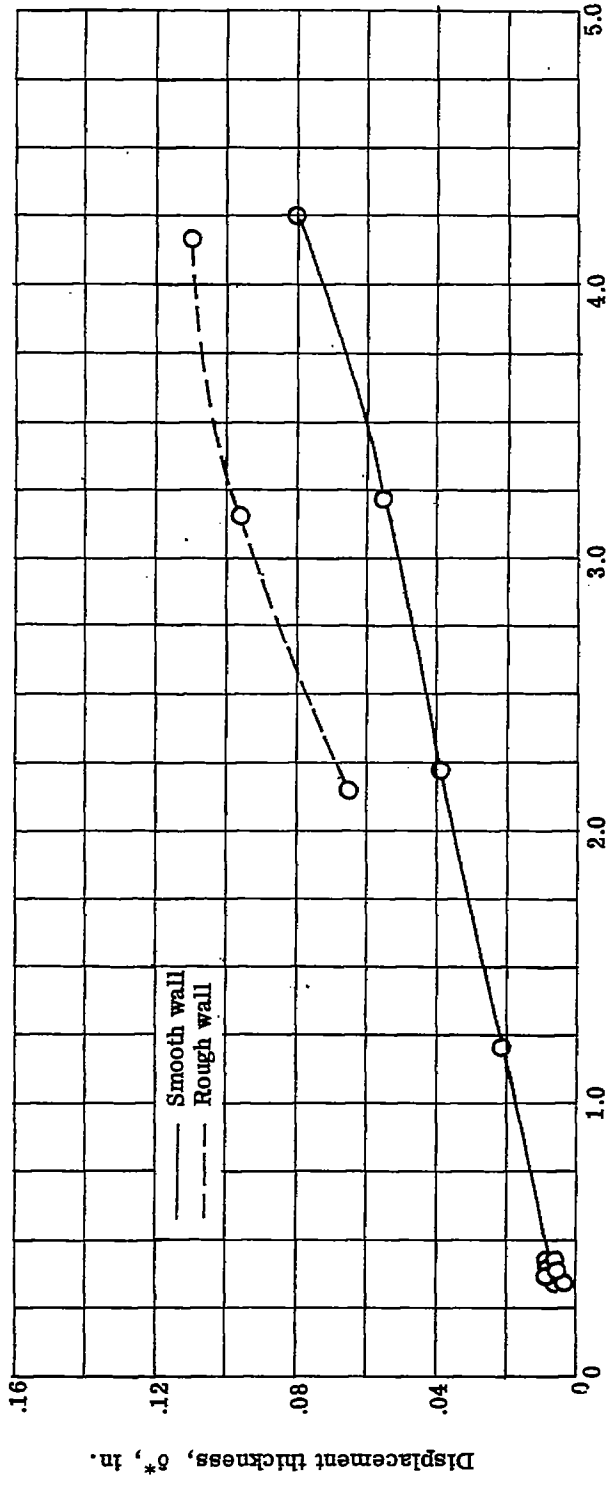

(b) Displacement thickness δ^*.

Figure 18.- Continued.

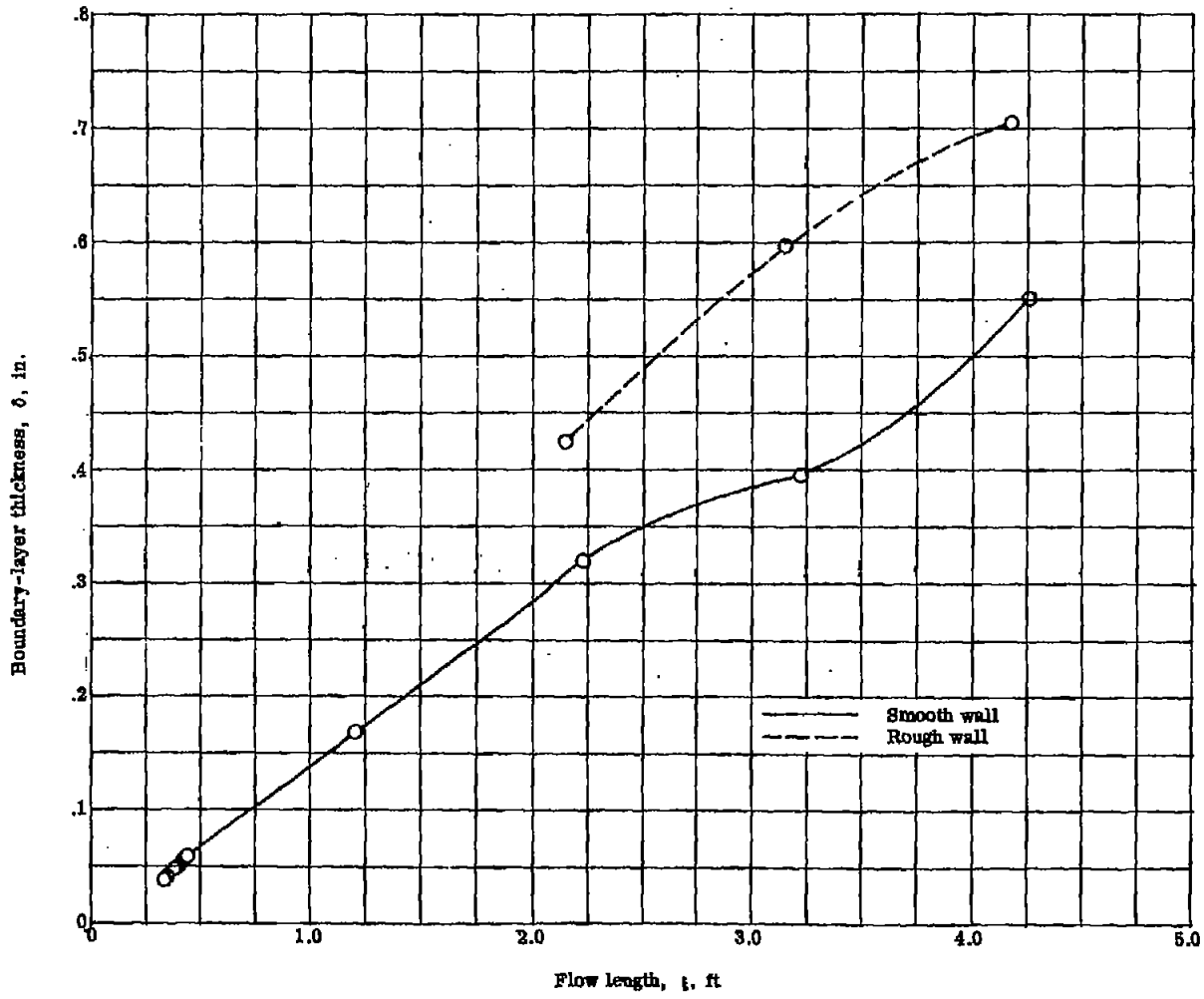

(c) Boundary-layer thickness δ.

Figure 18.- Continued.

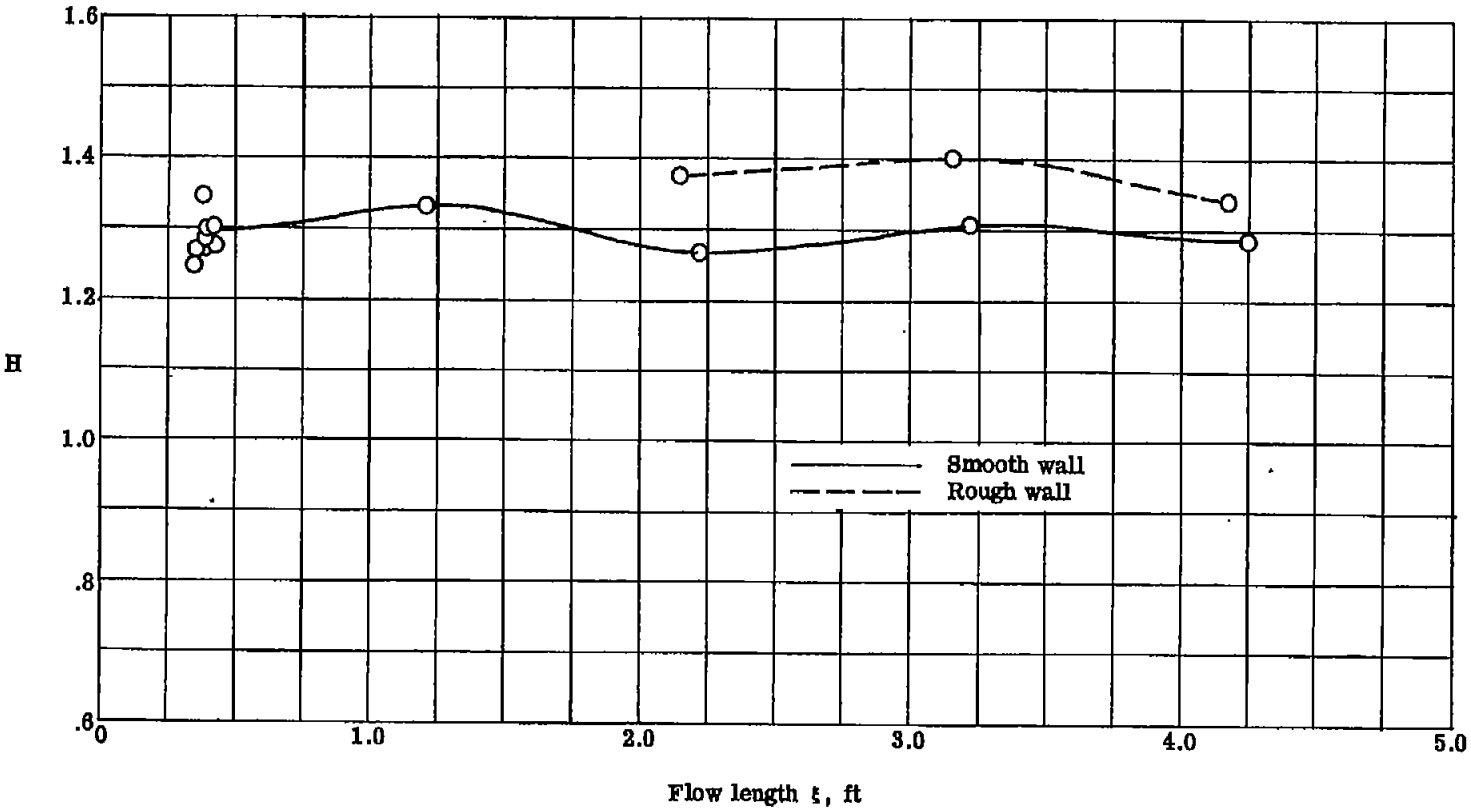

(d) Form parameter H.

Figure 18.- Concluded.

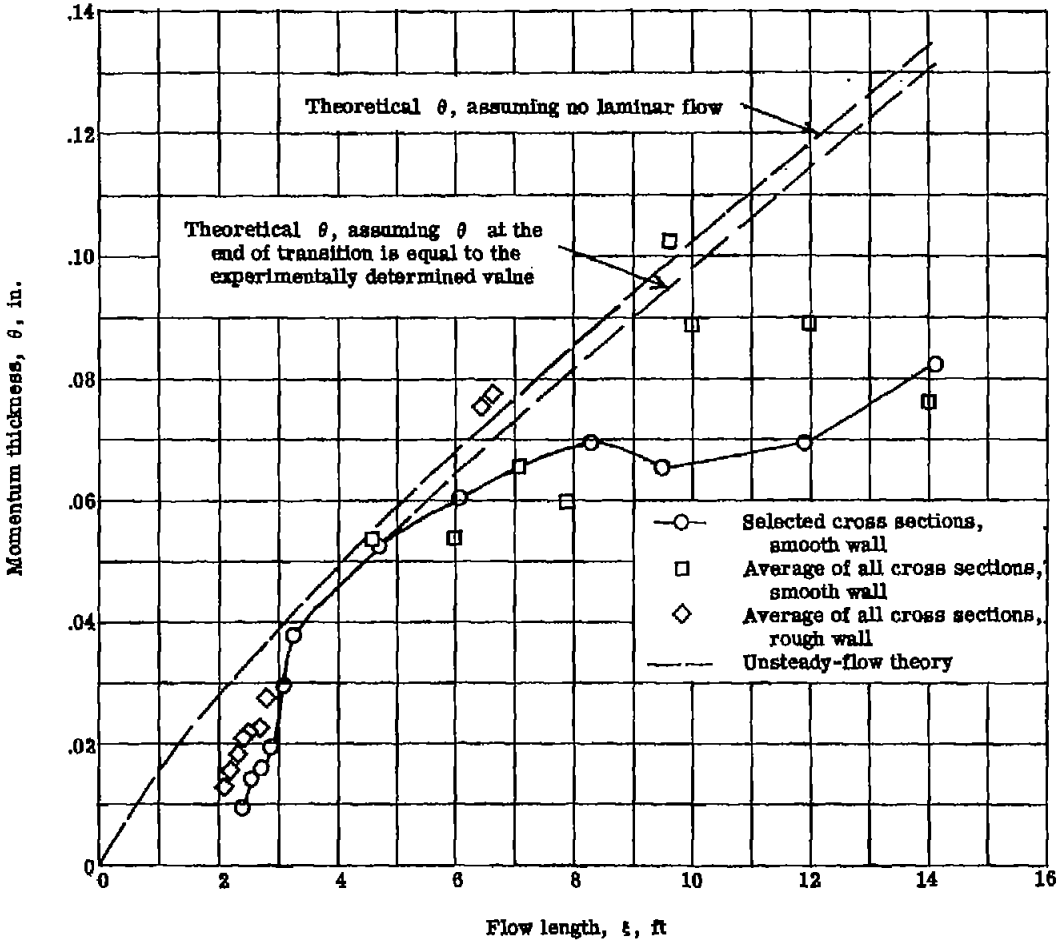

(a) Momentum thickness θ.

Figure 19.- Variation of various average flow parameters with free-stream flow length for M_2 = 1.77. Rough and smooth walls.

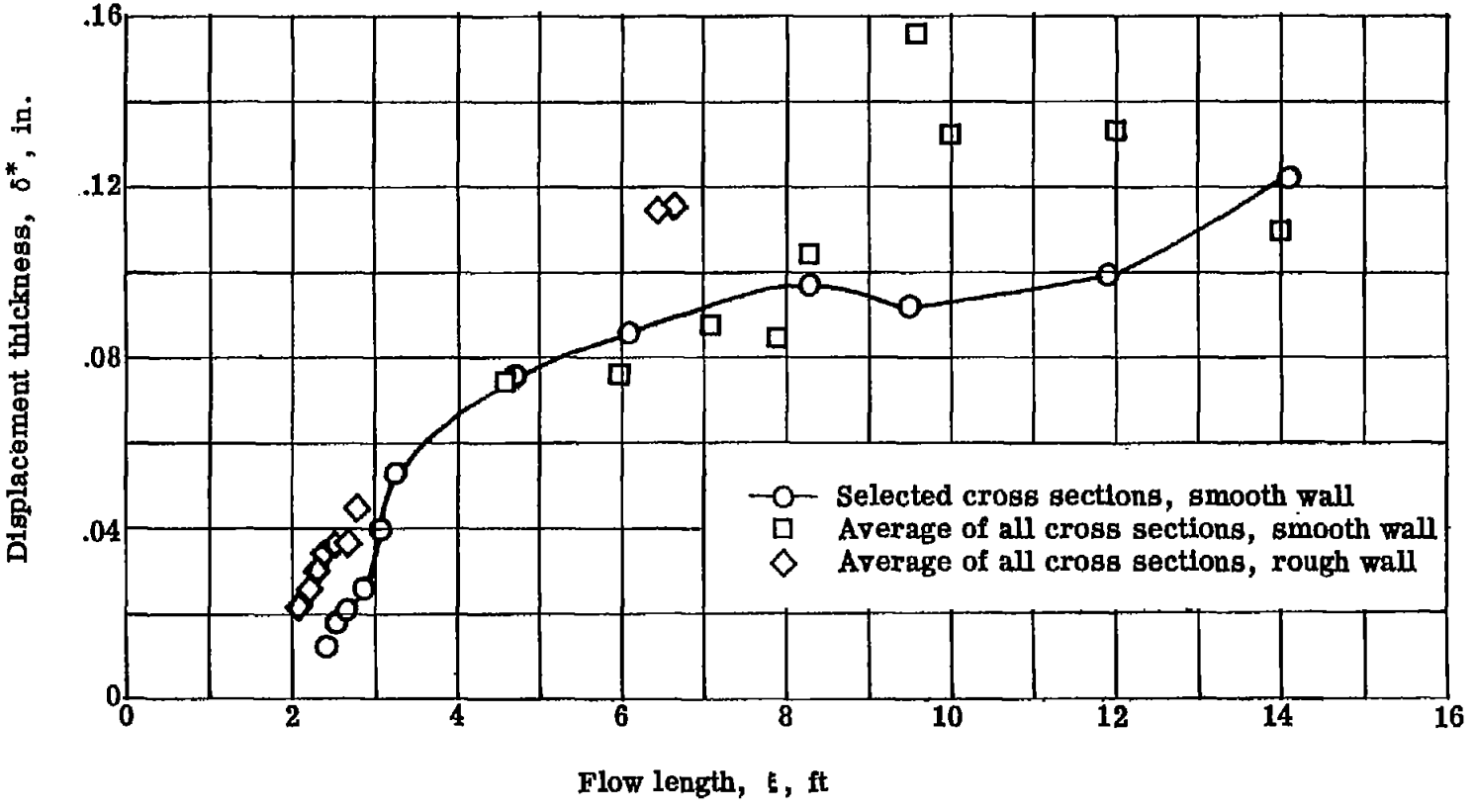

(b) Displacement thickness δ^*.

Figure 19.- Continued.

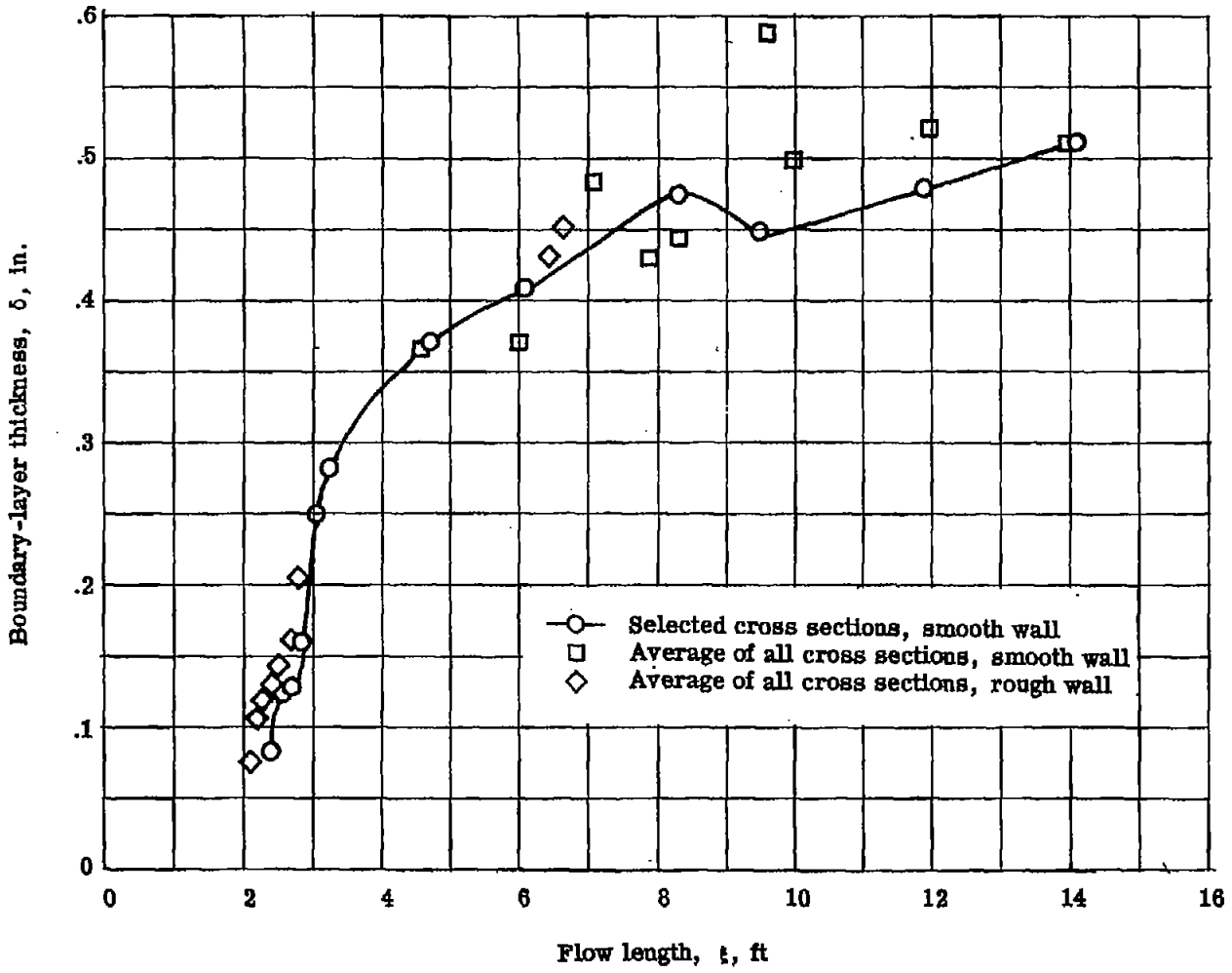

(c) Boundary-layer thickness δ.

Figure 19.- Continued.

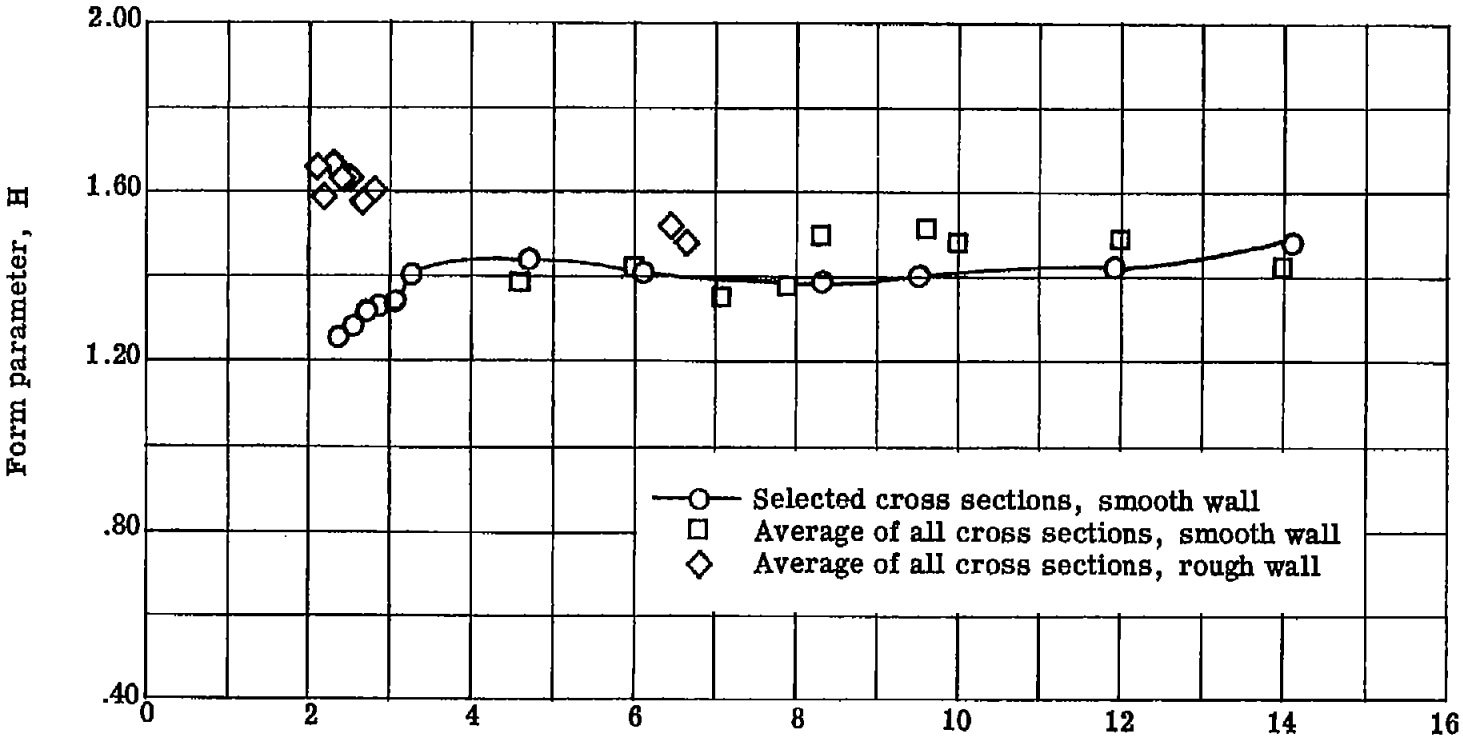

(d) Form parameter H.

Figure 19.- Concluded.